COHERENT OPTICAL ADAPTIVE TECHNIQUES (COAT)

S. Hansen, et al

Hughes Research Laboratories

Prepared for:

Rome Air Development Center
Defense Advanced Research Projects Agency

October 1973

AD-776 814

UNCLASSIFIED

SECURITY CLASSIFICATION OF THIS PAGE (When Data Entered)

REPORT DOCUMENTATION PAGE		READ INSTRUCTIONS BEFORE COMPLETING FORM
1. REPORT NUMBER RADC-TR-74-38	2. GOVT ACCESSION NO.	3. RECIPIENT'S CATALOG NUMBER
4. TITLE (and Subtitle) Coherent Optical Adaptive Techniques (COAT)		5. TYPE OF REPORT & PERIOD COVERED Interim 26 Jun to 26 Sep 73
		6. PERFORMING ORG. REPORT NUMBER Tech. Report No. 2
7. AUTHOR(s) S. Hansen, S. Lazzara, T. Walsh L. Horwitz, T. O'Meara, W. Bridges R. Kubo, J. Pearson		8. CONTRACT OR GRANT NUMBER(s) F30602-73-C-0248
9. PERFORMING ORGANIZATION NAME AND ADDRESS Hughes Aircraft; Hughes Research Labs 3011 Malibu Canyon Road Malibu, Calfi. 90265		10. PROGRAM ELEMENT, PROJECT, TASK AREA & WORK UNIT NUMBERS PE: 3E20 JON: 12790016
11. CONTROLLING OFFICE NAME AND ADDRESS DARPA 1400 Wilson Blvd Arlington, Va. 22209		12. REPORT DATE October 73 13. NUMBER OF PAGES 86
14. MONITORING AGENCY NAME & ADDRESS(if different from Controlling Office) Rome Air Development Center (OCTM) Griffiss AFB, NY 13441		15. SECURITY CLASS. (of this report) UNCLASSIFIED 15a. DECLASSIFICATION/DOWNGRADING SCHEDULE

16. DISTRIBUTION STATEMENT (of this Report)
Approved for public release. Distribution Unlimited.

17. DISTRIBUTION STATEMENT (of the abstract entered in Block 20, if different from Report)

18. SUPPLEMENTARY NOTES
R.F. Ogrodnik
OCTM
AC315 330-4306

19. KEY WORDS (Continue on reverse side if necessary and identify by block number)
Laser Phased Array
Adaptive Aperture
Atmospheric Turbulence Compensation

20. AUSTRACT (Continue on reverse side if necessary and identify by block number)
This report covers the fabrication phase of an experimental program to design, fabricate and evaluate an eighteen-element, self-adaptive, laser phased array. Computer simulation efforts were extended to aid in designing system electronics and in analyzing servo-loop performance for rapid glint selection and adaptive array focusing. The hardware configurations for the beamsplitter-mirror assembly (Phasor matrix), electronics and (cont.)

DD FORM 1 JAN 73 1473 EDITION OF 1 NOV 65 IS OBSOLETE

UNCLASSIFIED

SECURITY CLASSIFICATION OF THIS PAGE (When Data Entered)

Block 20. Abstract (cont.)

receiver/transmitter channels are described in this report along with the construction progress of the multiglint target hardware and propagation range instrumentation. A revised calibration and measurements program is described which reflects a 3-month delay in the completion of system electronics.

COHERENT OPTICAL ADAPTIVE TECHNIQUES (COAT)

S. Hansen
L. S. Horwitz
R. M. Kubo
S. P. Lazzara
T. R. O'Meara
J. E. Pearson
T. J. Walsh

Contractor: Hughes Research Laboratories
Contract Number: F30602-73-C-0248
Effective Date of Contract: 27 March 1973
Contract Expiration Date: 26 March 1974
Amount of Contract: $249,648.00
Program Code Number: 3E20

Principal Investigator: W. B. Bridges
Phone: 213 456-6411

Project Engineer: Robert F. Ogrodnik
Phone: 315 330-4306

This research was supported by the Defense Advanced Research Projects Agency of the Department of Defense and was monitored by Robert F. Ogrodnik RADC (OCTM), GAFB, NY 13441 under Contract F30602-73-C-0248.

FOREWORD

This quarterly report was prepared by Hughes Research Laboratories, Malibu, California, under Contract No. F30602-73-C-0248. It describes work performed from 26 June to 26 September 1973. The principal investigator and principal scientist is Dr. William B. Bridges.

SUMMARY

The first quarter of the program was devoted primarily to design studies for the prototype visible COAT system and to the initial checkout of a computer simulation for that system. The second quarter has been spent in final design adjustments, hardware construction, and further computer simulation studies. All of the required components have been received and, with the exception of the electronics, will be fully assembled and operational by mid-December, 1973. Delays in delivery of key electronic components has delayed completion of the entire system from the original goal of October 1, 1973 until early December.

A detailed analysis of the COAT servo-control system has been performed. The study has led to an increased understanding of the influence of filter characteristics, dither frequencies, loop gain, modulation index, and number of channels on the stability and convergence time of multidither outgoing-wave COAT systems. Some of the results of the study have been included in the final choice of parameters for the electronics of the prototype system. To date this analysis has been done on internal IR&D at Hughes Research Laboratories using a specialized digital computer simulation.

The complete computer simulation which includes transmitter and target characteristics has now been expanded to include trapezoidal transmitter elements and linear relative motion of the target glints. Several "animated movies" have been made using this simulation which graphically demonstrate the convergence of a COAT system on the stronger of two glints even when one is moving.

A number of refinements in the system electronics have improved the component performance and increased the versatility of the system. A new driver amplifier for the dither phase shifters has been developed to provide up to ±100 V with flat response up to 40 kHz. When driven by these amplifiers, the PZT cylinders chosen for the dither phase shifters will provide up to $\pm 60^{\circ}$ of phase modulation amplitude. A system of oscillators and phase shifters has been designed so that up to three channels can be driven with one frequency with the phase between channels continuously adjustable from 0° to 360°.

Preceding page blank

A sample-and-hold, slew-and-offset system has been built which will allow the COAT system, after it has locked onto a glint, to be scanned to a programmable point on the target for a selectable amount of time before returning to the original lock point. The scanning can be periodic at variable sample and hold times, and the system has the capability of using either electronic offset or microslewing mirrors to perform the slew/offset function.

A glint target has been designed and is under construction. The target can provide up to 4 glints with variable relative positions and reflectivities. Relative glint motion is provided by a moving mirror system. The target range setup is nearly complete. The range design includes adequate provisions for range safety and three separate instruments for monitoring atmospheric turbulence.

Because of the delays caused by component delivery, the measurements schedule has been revised. Less time will be spent on system calibration so that measurements on the GSG propagation range can begin in late December 1973, or early January, 1974.

PUBLICATION REVIEW

This technical report has been reviewed and is approved.

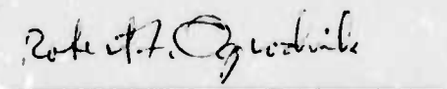

Robert F. Ogrodnik
RADC Project Engineer

TABLE OF CONTENTS

Pages vii AND viii
blank

LIST OF ILLUSTRATIONS

I. INTRODUCTION

A. Program Objectives

There are two primary objectives of this program. The first objective is to determine the performance limits of coherent optical adaptive techniques through operation of an experimental, visible prototype COAT system through a representative turbulent atmosphere against a complex dynamic target. The second objective is to determine the best methods of employing COAT in high power laser systems and to assess the status of necessary key high power components.

B. Revised Research Program Plan

The current fabrication phase of this program has encountered unavoidable delays in delivery of key hardware. As a result, the program plan shown in Technical Report No. 1 of this contract has been modified to that shown in Fig. 1.

C. Organization of This Report

The first quarterly report on this contract covered the design and analysis tasks from 1 April 1973 to 1 July 1973. This report covers the hardware construction phase of the program from 1 July 1973 to 1 October 1973.

Section II continues the computer analysis which was first discussed in the previous report. A new and specialized computer code has been developed using HRL funds to answer critical questions about the design and performance of nonlinear COAT servo systems. The final system design parameters derived from this program are presented. Results from the complete computer simulation are also presented showing the system dynamic convergence behavior with both stationary and moving targets.

Section III details the progress of the system hardware construction. Included are descriptions of the phasor matrix, phase shifters, electronic components, and optical receiver hardware. The progress on target and range fabrication and instrumentation is also discussed. The completion of

the hardware construction has been delayed by 8 to 12 weeks because of long delivery times on key electronic components.

Section IV describes the measurements program and the priorities in view of the reduced time for this phase of the program. Section V describes plans for the next quarter.

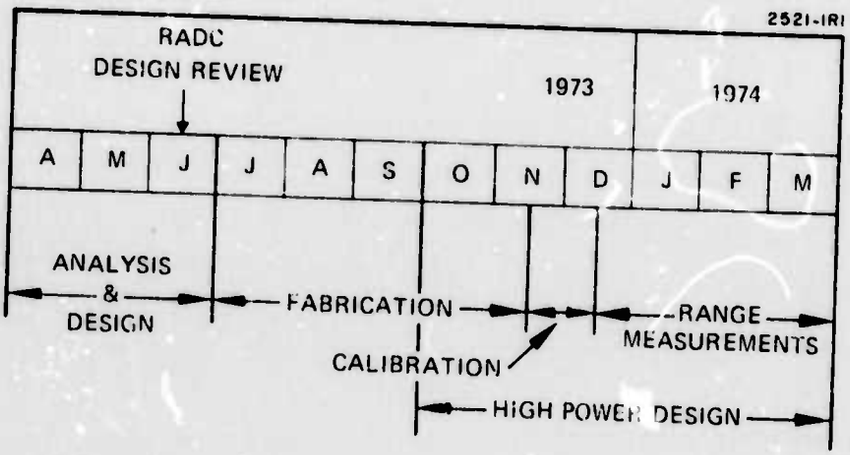

Fig. 1. COAT tasks and revised scheduling.

II. ANALYSIS

A. COAT Servo Loop Simulation

1. Philosophy of the Simulation

Part of the analytical task of this contract has been the development of a detailed computer simulation of a COAT system which would model all elements of the transmitter and receiver and the propagation path. The computer code has been developed and is operated by the Hughes Ground Systems Group (GSG). The initial results from this simulation are discussed in Technical Report No. 1 of this contract and more recent results are detailed later in this report.

Although the GSG computer code has the capability to vary all important COAT system parameters, it was realized early in this contract that a more elementary code could be of great value for studying servo-loop control problems. A simple computer code was developed to model just the COAT nonlinear control system. This work has been done as part of the Internal Research and Development program at Hughes Research Laboratories (HRL). The goals of this phase of the analytical task are as follows:

1. Detail the behavior of a multidither COAT control system to provide data for understanding how various parameters affect the convergence time, final converged state, and stability of the system.

2. Perform an optimization study on various system parameters with the goal of optimizing the performance of the 18-element system under construction on this contract.

Table I lists the parameters which are of interest in a simulation of a COAT control system. Some of the quantities such as the phase shifter resonance and the dither band location are set by the elements of the system being simulated. Still, an exhaustive study of the range of all the other parameters would require a very large number of computer runs.

TABLE I

COAT Control System Parameters

1.	Phase shifter resonance frequency and resonance Q.
2.	Number of channels
3.	Low-pass filter design
	a. Number of stages
	b. Corner frequencies
4.	High-pass filter design
	a. Number of stages
	b. Corner frequencies
5.	Dither bandwidth
6.	Dither band location
7.	Dither frequencies
8.	Dither phase angles
9.	Dither modulation amplitude
10.	Open loop gain
11.	Photomultiplier shot noise
	a. Noise bandwidth
	b. Signal-to-noise ratio

T1113

The large number of possible parameter choices leads to an interactive approach to parameter optimization. First, criteria for optimum performance in the presence of noise are chosen. These criteria are (1) rapid convergence, (2) high level of final convergence, and (3) the absence of slow modulation on the converged value which would indicate the onset of servo

instability. Next, starting from some selected set of parameter values, one parameter is varied to find a local performance optimum with respect to that variable. The process is then repeated with each variable. This procedure does not guarantee an absolute optimum set of parameter values, but in practice will result in a set giving acceptable, if not quite optimum, performance.

2. Simulation Procedure

The simulation approach modeled each element of the servo loop in terms of a network of integrators, summers, multipliers, etc. This is a standard technique in the use of analog computers and is equivalent to writing the coupled, first-order, linear differential equations for each network element which relate the output of the device (e.g., a filter) to its input. All of the elements are then linked together to form the closed servo loop. Digital computer techniques are used to solve the resulting set of simultaneous differential equations.

The size of the simulation code has progressed from a simple two-channel system with one filter stage per channel to the present 18-channel system shown in Fig. 2. The present code includes up to 18 channels, each of which has a sine-wave multiplier for detection, a 5-stage adjustable low-pass filter, a phase-shifter resonance, and provision for initial biases on the phase-shifter. There are no provisions for transmitter array parameters or complex targets; the "optical path" is equivalent to putting the detector behind a single glint located on boresight. The receiver has a shot noise simulation, a 2-stage high-pass filter and a gain parameter for adjusting the open-loop gain (no AGC option). The number of channels as well as all the various parameters can be varied. The complete 18-channel system is equivalent to 130 simultaneous coupled differential equations.

A typical run using this code covers 5 msec of simulated time and includes 1000 steps at intervals of 5 μsec. The program provides a graphical output showing intensity on the glint as a function of time and printed output of the relative phases of the bias phase shifters at 25 intervals during the run. A typical result showing "optimum" system performance without noise is shown in Fig. 3. The ordinate axis is the intensity on the glint as a percentage

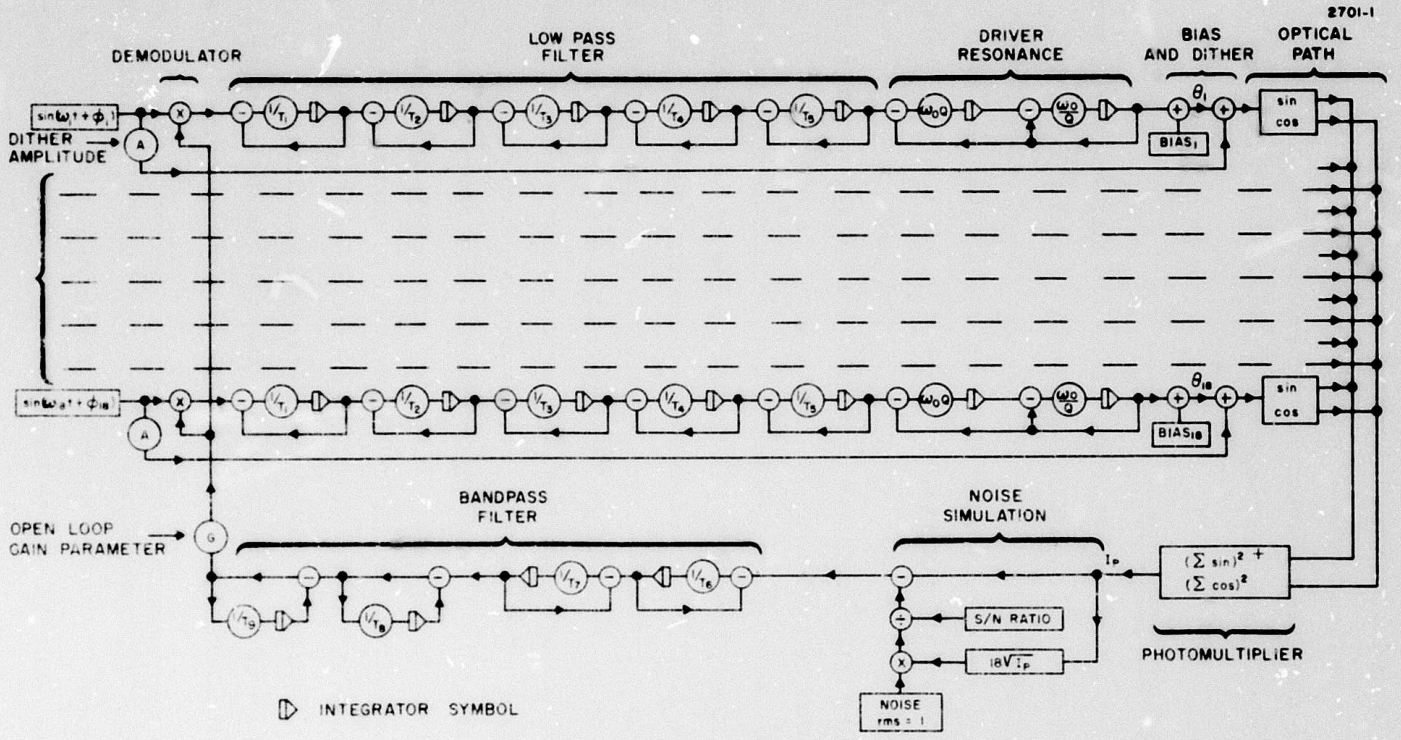

Fig. 2. Schematic of COAT servo-loop simulation.

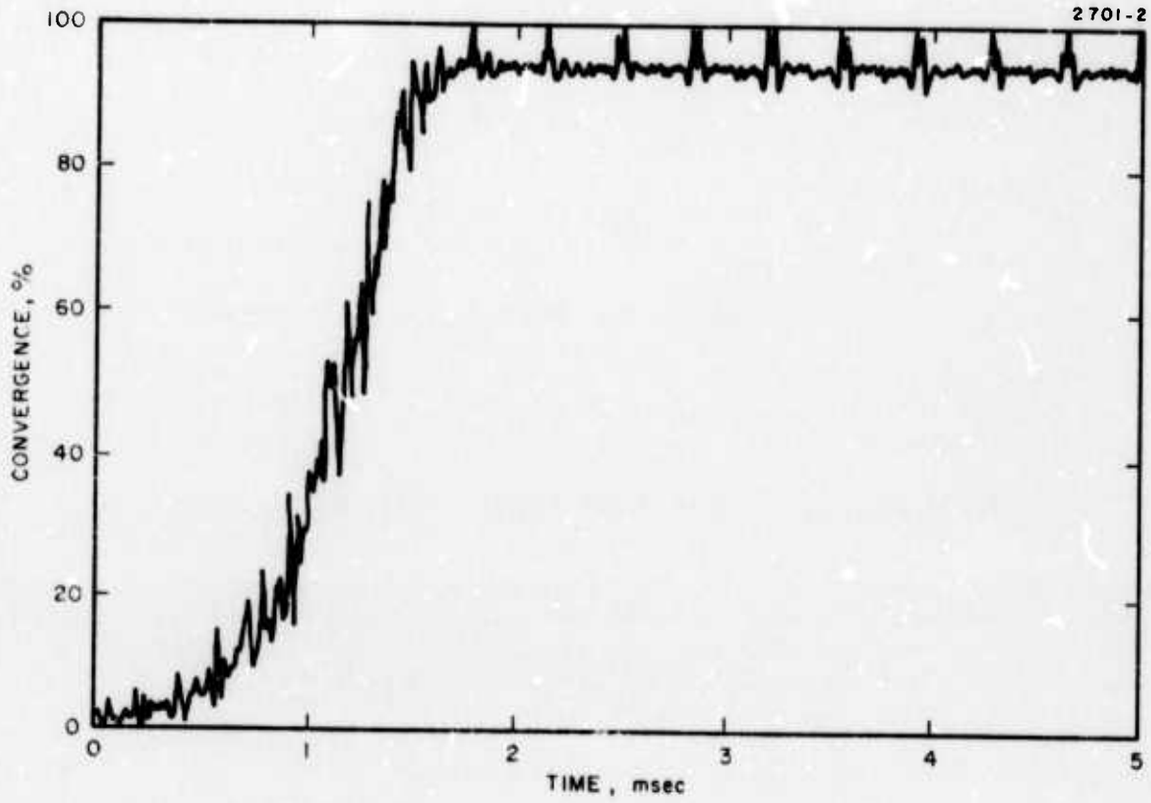

Fig. 3. "Optimum" noise-free servo-loop performance.

of the maximum possible. The periodic oscillations of the intensity up to 100% convergence are an artifact of having all the dither oscillators start at the same instant of time; they disappear when random initial starting times are used. The "optimum" performance criteria for this case (signal-to-nose is infinite) are shown in Table II.

TABLE II

Noise-Free "Optimum" Servo-Loop Performance for 18 Channels

Open-loop gain	35 dB
Final converged value	94% of maximum
Convergence time (initial 3 to 94% final value)	1.6 msec
Convergence time (10% to 90% of final value)	0.8 msec
Servo-loop instability oscillations:	None

T1114

The open-loop gain for this simulation is defined by

$$OLG = (N-1)G \sin(A) \qquad (II-1)$$

where N is the number of channels, G is the open loop gain parameter (electronic), and A is the dither modulation amplitude. The servo parameters which lead to the results of Fig. 3 and Table II are discussed in the following section.

3. Simulation Results - Nonlinear Servo Performance

A number of interesting servo loop phenomena have been identified. The first of these is a peculiar form of instability which causes the system to plunge from almost full convergence to no convergence in less

than one dither cycle. The abrupt nature of the instability led to its being termed "crashing." An example of this type of behavior is shown in Fig. 4.

The onset of crashing occurs abruptly as the open-loop gain is increased. Careful investigation of the signals existing throughout the loop showed that a regenerative amplification of the dither fundamental caused a very large dither signal to appear at the output of each low-pass filter. The remedy for this type of instability was simply to modify the filtering to suppress the unwanted dither signals.

Another potential source of servo instability is the mechanical resonance of the bimorph phase shifters. As indicated in Technical Report No. 1 of this contract, the resonance is near 14 kHz with a Q of 20. It was found that a four-stage low-pass filter with each corner at 5 kHz would perform the two functions of rejecting unwanted dither frequencies and suppressing the bimorph resonance. The multistage low-pass filter is preferable to the earlier choice of a notch filter for suppressing the bimorph resonance since drifts in either the notch filter center frequency or the mechanical resonance frequency could have led to servo instability; with the new filter design, such drifts will have no effect on system performance.

Another important area of study has been the selection of dither frequencies and phases. As indicated in earlier COAT reports, an economy of dither frequencies could be effected by operating two channels with the same frequency, but with 90° phase difference between channels. This has been termed "sine-cosine" operation.

Originally it was believed that the various channels need to be nearly independent of each other so that relative phases of other than 90° for two channels, or more than two channels per frequency would not be possible. This assumption has been proven incorrect, although 90° phase difference and two frequencies per channel has proven to be near the optimum. Any relative phase between two channels operating on the same frequency will work, even 180°, and the COAT system is insensitive to relative phase shifts which might be introduced between channels. Thus, a nominally sine-cosine system will work with equal effectiveness if the relative phase between channels is between 70° and 110°. This fact eliminates what had been feared to be a potential deficiency of sine-cosine operation: the necessity of accurate phasing of the two channels. We have also studied systems which use three

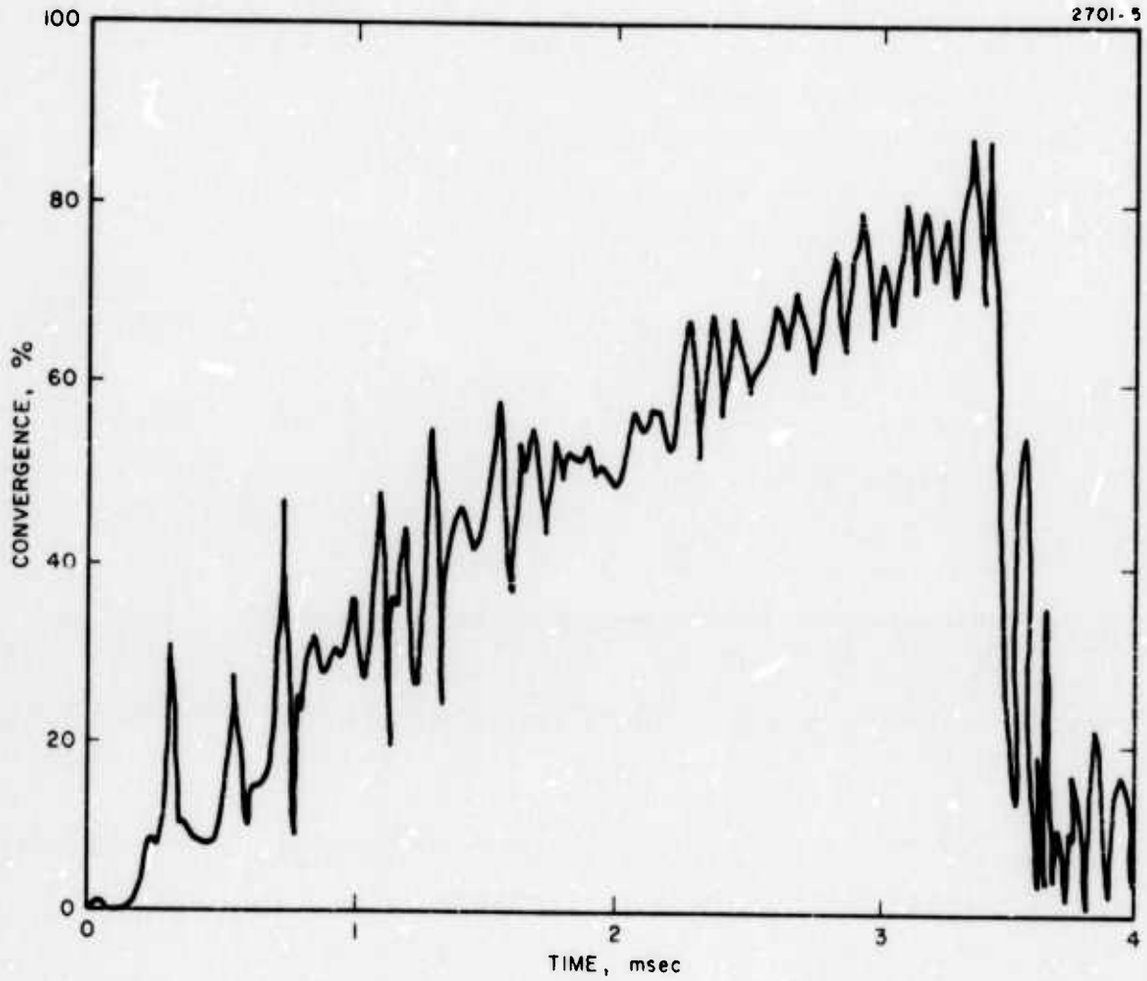

Fig. 4. "Crashing" type of servo instability.

frequencies per channel, but not exhaustively. We intend to continue to study promising aspects of this approach.

Increasing the number of channels in the system, say from 9 to 18, has not resulted in any discernible change in performance as long as the open loop gain is scaled according to eq. (1), and as long as the dither frequency spacing is maintained above a certain minimum (see next section). It is still possible, however, that there are important effects whose influence increases as the number of channels increases. For this reason, 18 channels were used in all of the parameter optimization runs discussed in the next section.

4. Simulation Results - Parameter Optimization

Of the parameters listed in Table II, items 1, 2, 5 and 6 are set by the system now under construction. The number of channels is 18 and the bimorph phase-shifter resonance is at 14 kHz with a Q of 20. The PZT cylinders used for the dither phase shifter can be used effectively only up to 32 kHz (see Section III). This limit plus the low-pass filter corner at 5 kHz dictate a dither bandwidth and band location of 8 kHz to 32 kHz.

Contrary to earlier expectations, this study has shown that no detrimental effects occur by choosing a dither bandwidth greater than one octave if the filter designs are correct even if a dither frequency is the second harmonic of another. For an 18-frequency system and a 32 kHz dither band, the maximum dither frequency separation is 1.4 kHz, an acceptable although probably not an optimum value.

Channel frequency separation, Δf, has been studied in some detail. We have concluded that convergence time is not affected as Δf is reduced if the loop gain is constant. The system becomes less stable with decreasing Δf, however, unless the open loop gain is reduced; the lower gain then increases the convergence time. This effect is quite noticeable for $\Delta f \lesssim 1.4$ kHz and becomes intolerable for $\Delta f \leq 1.0$ kHz.

Sine-cosine operation was originally conceived as a solution to the problem of trying to increase the number of dither frequencies in a fixed bandwidth. Sine-cosine operation has been shown to be superior to one frequency per channel if the total dither bandwidth is kept constant (Δf is thus doubled), but it is inferior if Δf is held fixed. It is estimated that sine-cosine

operation can increase the number of available dither frequencies in a fixed bandwidth by no more than $\sqrt{2}$ for performance equal to a one frequency per channel system. For the rest of the parameter studies, sine-cosine operation with $\Delta f = 2.8$ kHz is selected as the optimum choice.

The filter characteristics have proven to be the most critical parameters in the COAT servo system. As previously discussed, stability studies indicated the choice of a 4-stage low-pass filter with corner frequencies at 5 kHz. A fifth stage with a very low corner frequency has also proved beneficial. This stage has the effect of enhancing the dc gain of the loop and thus improves the degree of final convergence as well as the convergence time. Our studies indicate 15 Hz as an upper limit for the corner frequency of this stage.

The design of the high-pass filter which follows the photomultiplier turns out to be uncritical. A bandpass filter with a lower cutoff at 1 kHz and an upper corner at 50 kHz has proven adequate to reject the dc component and limit the noise bandwidth while still passing all dither frequencies. In practice, the frequency response of the receiver electronics limits the high frequency response to near 50 kHz so that a two-stage high-pass filter is used.

The net loop frequency response for a conservative loop gain is shown in Fig. 5 along with the bimorph amplitude characteristic. Note that the filter design puts the bimorph resonance well below the unity gain level. The unity gain point for this choice of loop gain (29 dB) is roughly 400 Hz which would lead to a convergence time (10% to 90% of final value) of around 1.1 msec.

The simulation of photomultiplier shot noise has only recently been added to the computer code. The signal-to-noise ratio (S/N) is defined as the ratio of the dc photomultiplier signal at full convergence to the rms value of the noise. The noise is gaussian and is generated in such a way that it has a bandwidth of about 66 kHz.

Only a few runs have been made with the noise simulation routine in the code. Figures 6 and 7 illustrate the convergence of the system for two different gain values and a S/N = 20. The run shown in Fig. 6 has nearly optimum gain; the gain for Fig. 7 is one-half this value. As can be seen,

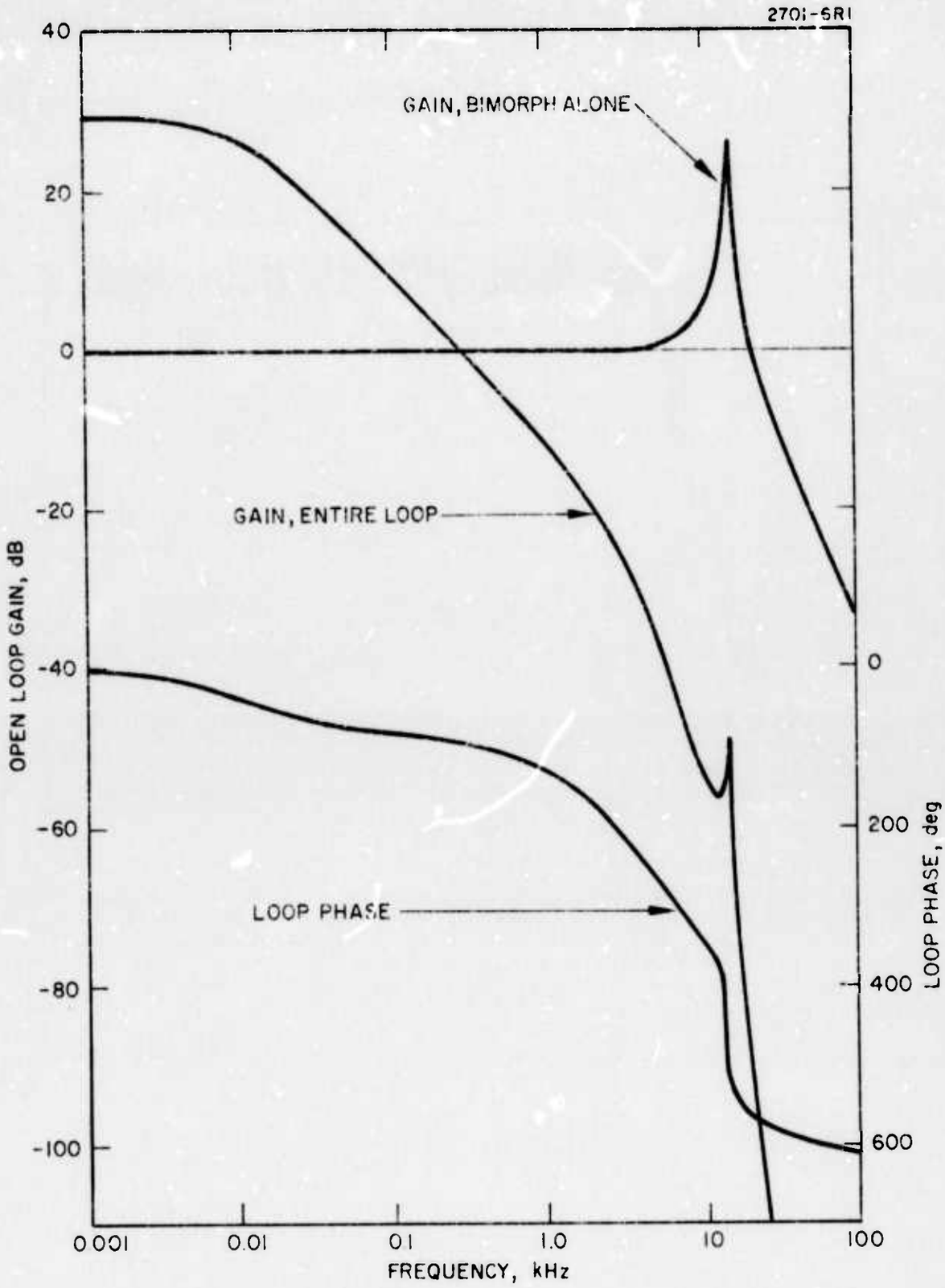

Fig. 5. Net open-loop frequency response for 29 dB open-loop dc gain. Also shown is amplitude response of bimorph alone.

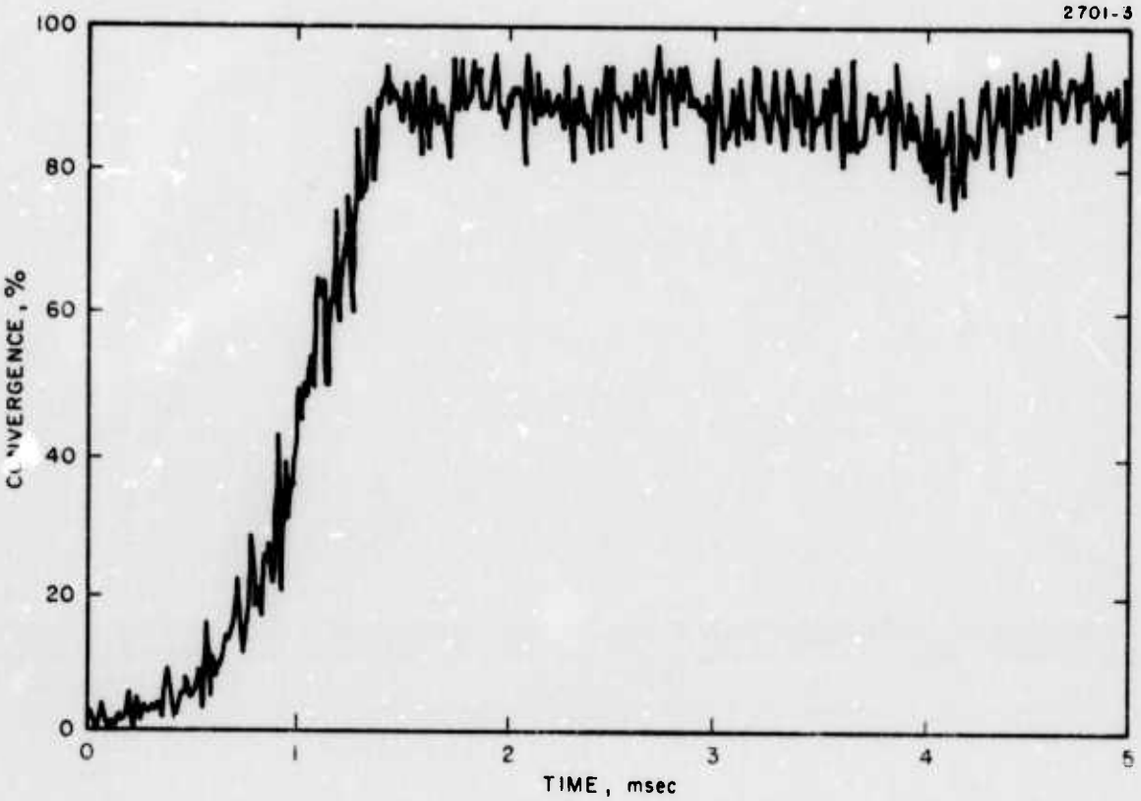

Fig. 6. Servo-loop response in the presence of noise (S/N = 20). Open-loop gain is near the optimum for minimum convergence time.

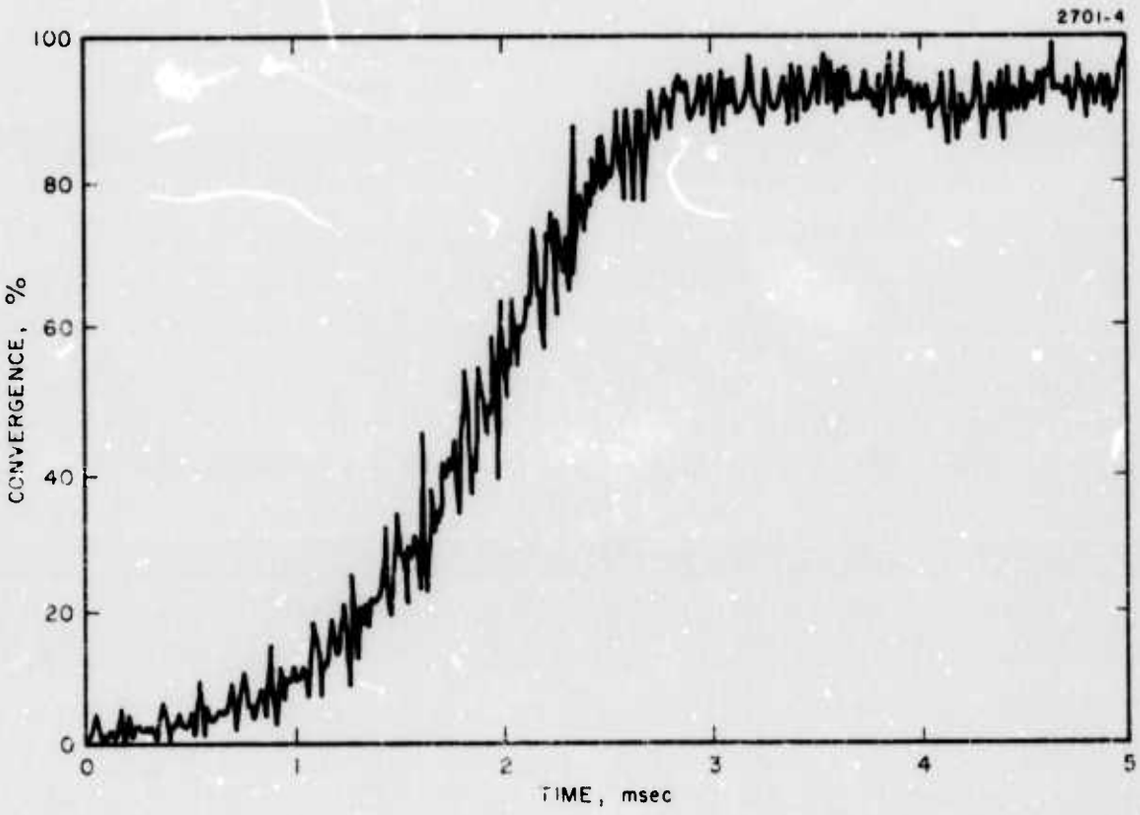

Fig. 7. Same as Fig. 6, but for one-half the open-loop gain. Note longer convergence time, but higher final convergence.

there is a trade-off between convergence time and the stability and level of final convergence. These runs should be compared with the noise-free case shown in Fig. 3.

The indication of the few runs that have been made with noise is that the 18-channel system will work adequately with a S/N ratio of about 20, but only if the gain is reduced by factor of 2 from its noise-free value. Such a gain reduction does, of course, increase the convergence time.

The presence of noise has a strong influence on the choice of dither modulation amplitude (modulation index). For a given S/N, there will be an optimum modulation index for maximum convergence. Figure 8 shows how the final convergence level varies with the modulation amplitude for different S/N values. For the noise-free case, the percentage convergence appears to vary as the cosine of the modulation amplitude. The general conclusion is that the dither amplitude should be as large as possible, consistent with an acceptable convergence level. A peak amplitude of 20° ($\pm 20^{\circ}$ swing) seems to be a good compromise.

As expected, the simulation has shown that higher gain results in a shorter convergence time. The small-signal gain of the system should thus be as high as possible, consistent with system stability. Figure 9 indicates the simulation results obtained with no AGC in the system; the convergence time varies approximately as the reciprocal of the open-loop gain.

The final parameter values chosen and incorporated into the system electronics hardware are shown in Table III. Some of the parameters such as dither frequency separation and dither modulation amplitude can still be varied, but the values in the table are expected to give optimum performance. The maximum open-loop gain will be determined experimentally and then controlled with an AGC system.

5. Plans for Additional Servo Loop Studies

There are two main questions about the COAT servo control loop which remain unanswered. First, what is the effect of an automatic gain control (AGC) on the control loop performance? Experimental studies with the HRL 7-element system showed a marked improvement in performance when an AGC was added. The electronics for the visible model has an

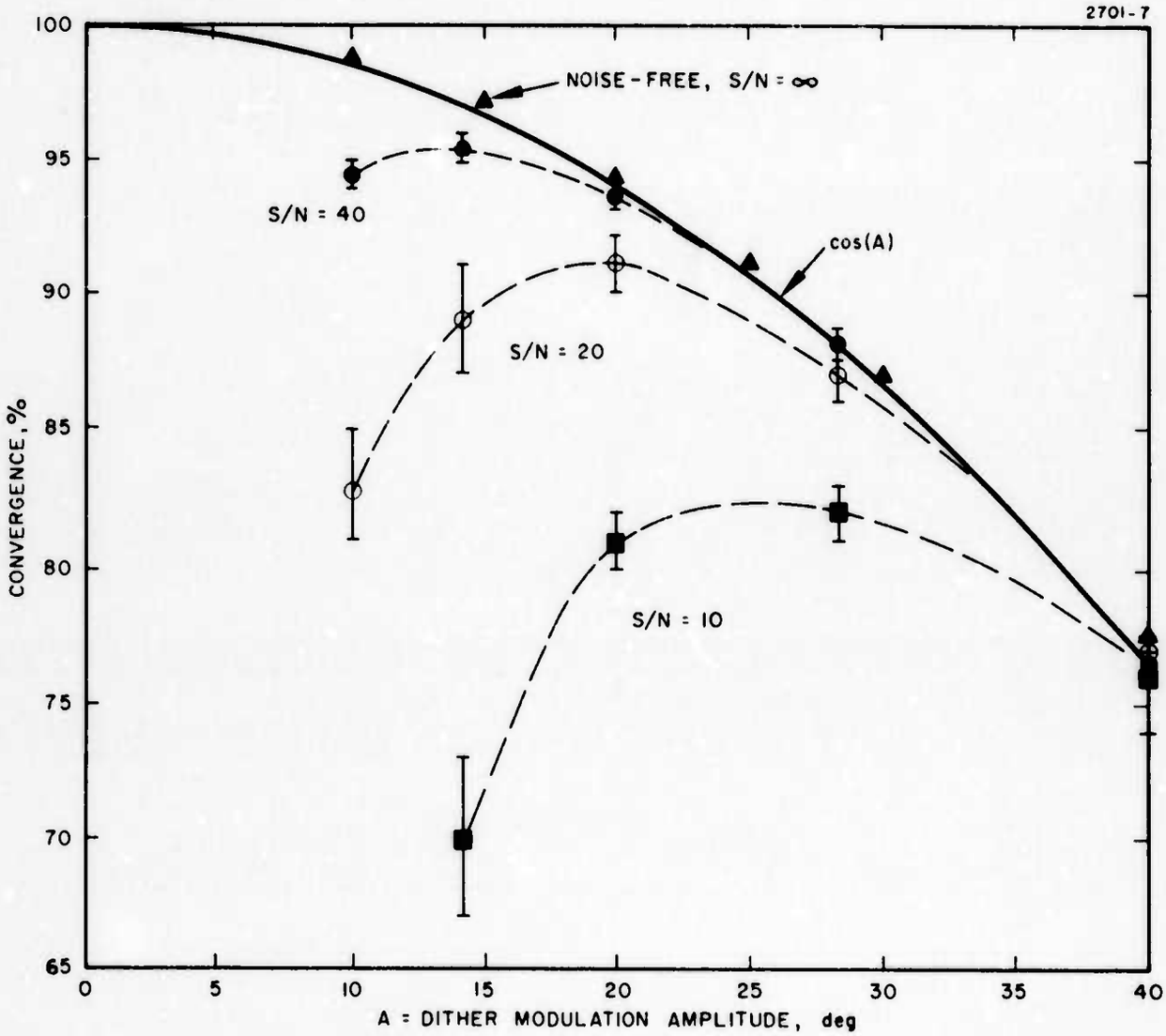

Fig. 8. Final convergence values for 18-channel servo as a function of dither modulation amplitude and signal-to-noise ratio.

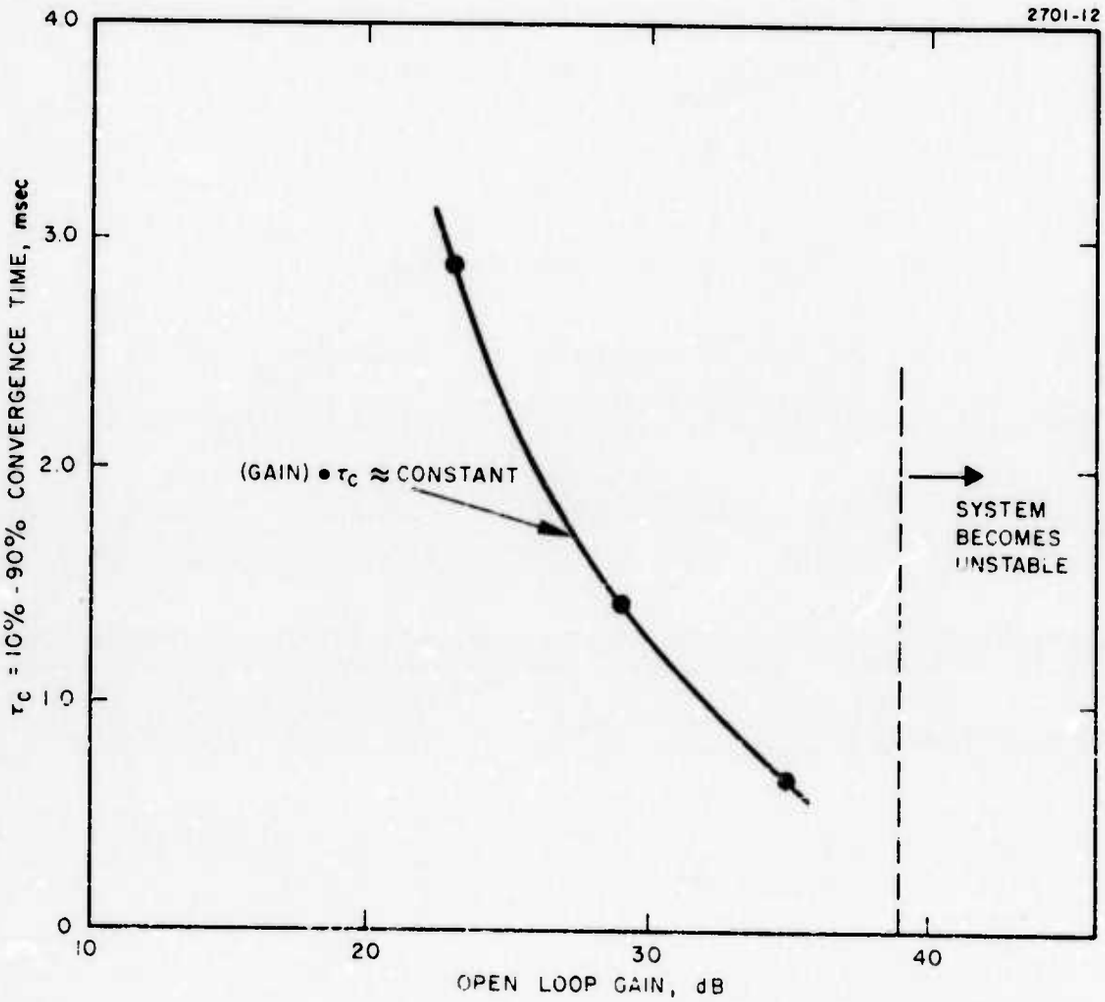

Fig. 9. 18-element system convergence time as a function of open-loop gain. No AGC is employed in the system.

TABLE III

Final COAT System Servo Parameter Values

1.	Phase shifter resonance: $f \approx 14$ kHz with $Q = 20$.
2.	Number of channels: 18.
3.	Low-pass filter: 5 stages. One corner frequency at 10 Hz, 4 at 5 kHz.
4.	High-pass filter: 2 stages with corners at 1 kHz.
5.	Dither bandwidth: 24 kHz.
6.	Dither band location: 8 kHz to 32 kHz.
7.	Dither frequencies: 8.2 kHz to 32 kHz with $\Delta f = 1.4$ kHz for 18 frequencies, 2.8 kHz for 9 frequencies (sine-cosine).
8.	Dither phase angles: 0° (18 frequencies), 90° (sine-cosine).
9.	Dither peak modulation amplitude: 20°.

T1115

AGC network designed into it as discussed later in this report and in the first quarterly report. The design of this AGC has not been optimized, however, and at the moment is identical to that used on the earlier 7-element system. We plan to model the current AGC design to determine its effects on system performance and then to optimize the design to improve the control loop performance.

The second unanswered question is how well does the computer code predict the actual servo loop performance? The appropriate comparisons will be made once the hardware system is operational. We can then assess the value of this type of computer simulation in designing nonlinear servo control loops and in predicting their performance.

B. COAT System Simulation

1. Accomplishments During the Second Quarter

Most of the features of the complete computer simulation were discussed in the previous quarterly report. The past quarter has been spent in improving the running speed of the program and in final debugging.

The capabilities of the simulation have been expanded greatly during the past three months. The code can now provide a variety of transmitter arrays and moving target configurations. A series of motion pictures have been made by photographing the time-evolving target plane power contour maps generated by the simulation. When the power contours are appropriately colored, the result is a graphic illustration of the COAT system's simulated performance. The details of the simulation results are discussed in the following sections.

2. Simulation Improvements

The subroutine for the transmitter array now has the capability of handling multi-ring arrays of trapezoidal elements. Previously, only square arrays and elements could be used. Given the array outside and inside diameters, the number of rings, and the number of elements, the subroutine computes the trapezoidal element dimensions, locations, and orientations. Arrays can be simulated for the following configurations: 0-6, 0-6-12, 0-6-12-18, 0-12, 0-12-18, and 0-12-18-24, where the numbers indicate the number of elements per ring. The last three possibilities enable simulation of practical cases where the central obscuration is so large that a 6-element ring is undesirable (element dimensions become too large).

The subroutine which computes the target plane power density contour map has been expanded to include one moving glint with up to nine stationary glints. The moving glint follows a straight line path across the target plane from selectable starting and ending points. Expansion of the subroutine to handle more than one moving glint is planned for the next quarter.

3. Simulation Results

Using a 0-6-12, 18-element transmitter array, three target configurations have been studied to date: One stationary glint, two stationary glints, and two glints with one moving. System parameters were chosen to correspond with the 18-element system being constructed, but recent design changes were not incorporated for the results discussed here. The low-pass filter, for example, was the earlier 2-stage unit with corner frequencies of 60 Hz and a notch filter for suppressing the bimorph resonances. The final design values are now being used and will only improve upon the performance discussed here.

The target plane power map is computed on a 101 x 61 point grid. The computed power at each point is assigned a code numeral from 0 to 3 depending upon its magnitude relative to the theoretical boresight maximum. The code used is shown in Table IV. The code number is printed by a line printer on standard paper to produce the power map. Because of normal character and line spacing (10 per inch horizontal, 6 per inch vertical), the result is a 10 in. x 10 in. plot. The sample point spacing is always chosen so that the 10 in. distance represents the null-to-null beamwidth of one transmitter element.

TABLE IV

Target Plane Power Plot Code

Digit	dB Down from Boresight Maximum
0	0 to -3
1	-6 to -9
2	-12 to -15
3	-18 to -21

T1116

A number of color motion picture sequences have been made as part of the GSG IR&D program. For these sequences, the contour codes shown in Table IV are also assigned a color which is put onto the computer generated contour plots by hand. The time development of the array pattern is then photographed like an animated movie by shooting 10 sec. sequences of each plot (roughly 20 plots per simulation run). After editing, the resulting film shows graphically how the COAT system forms up the array and tracks a moving target. Sequences from three of these films are discussed in the following paragraphs.

a. Single Stationary Target – Figure 10 illustrates the convergence of the 18-element 0-6-12 array on a single stationary glint. The glint is located in the first quadrant at the 3 dB level of an element pattern and the array has a "random" initial phase condition. Convergence occurs in about 1 msec and the peak power on the glint is slightly less than 3 dB down from the boresight maximum as evidenced by the blank area around the glint. Note that the inside of the ring formed by the numeral "1" is the -6 dB contour. In all of the runs with the 0-6-12 two-ring array, the array beamwidth is approximately one-fifth the element beamwidth.

b. Two Stationary Target – Figure 11 illustrates the convergence behavior for two glints, each placed on the element 3 dB pattern. Glint B is 5 dB stronger than glint A and the array is initialized to boresight convergence. The sequence of events for this run is as follows:

1. Maximum power on boresight axis (Fig. 11(a)).
2. Power begins to build on both glints (Fig. 11(b)-(f)).
3. The array converges to near the theoretical maximum on the larger glint B with little power on glint A or boresight. (Fig. 11(g)-(i)). Note the appearance of the grating lobe diametrically opposite glint B.

c. Two Targets, One Moving – Figure 12(a) indicates the randomized initial condition for this simulation. Glint A is stationary on the

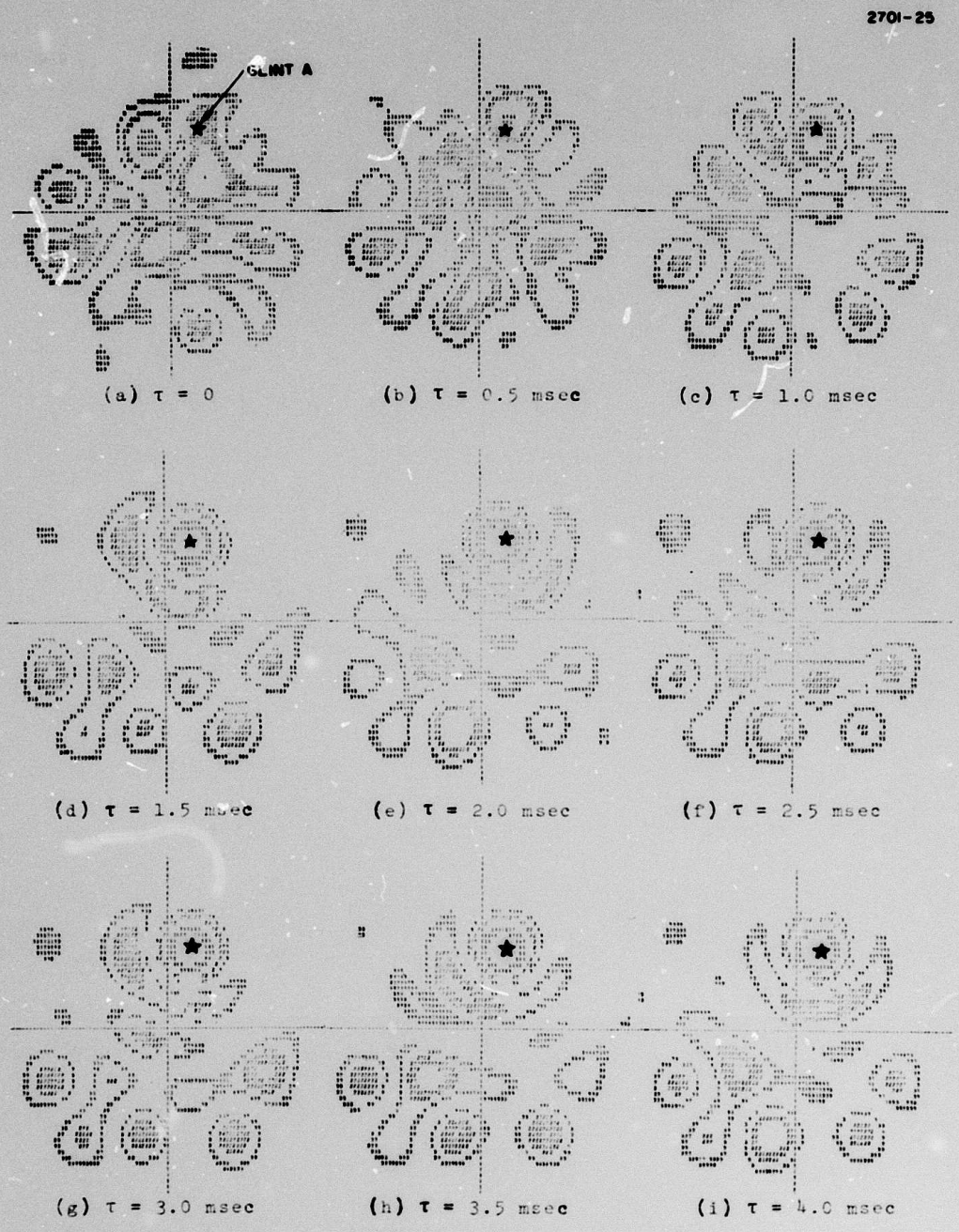

Fig. 10. Convergence sequence of 0-6-12 array for a single glint located on the element 3 dB contour. The COAT array starts from a "random" initial phase condition.

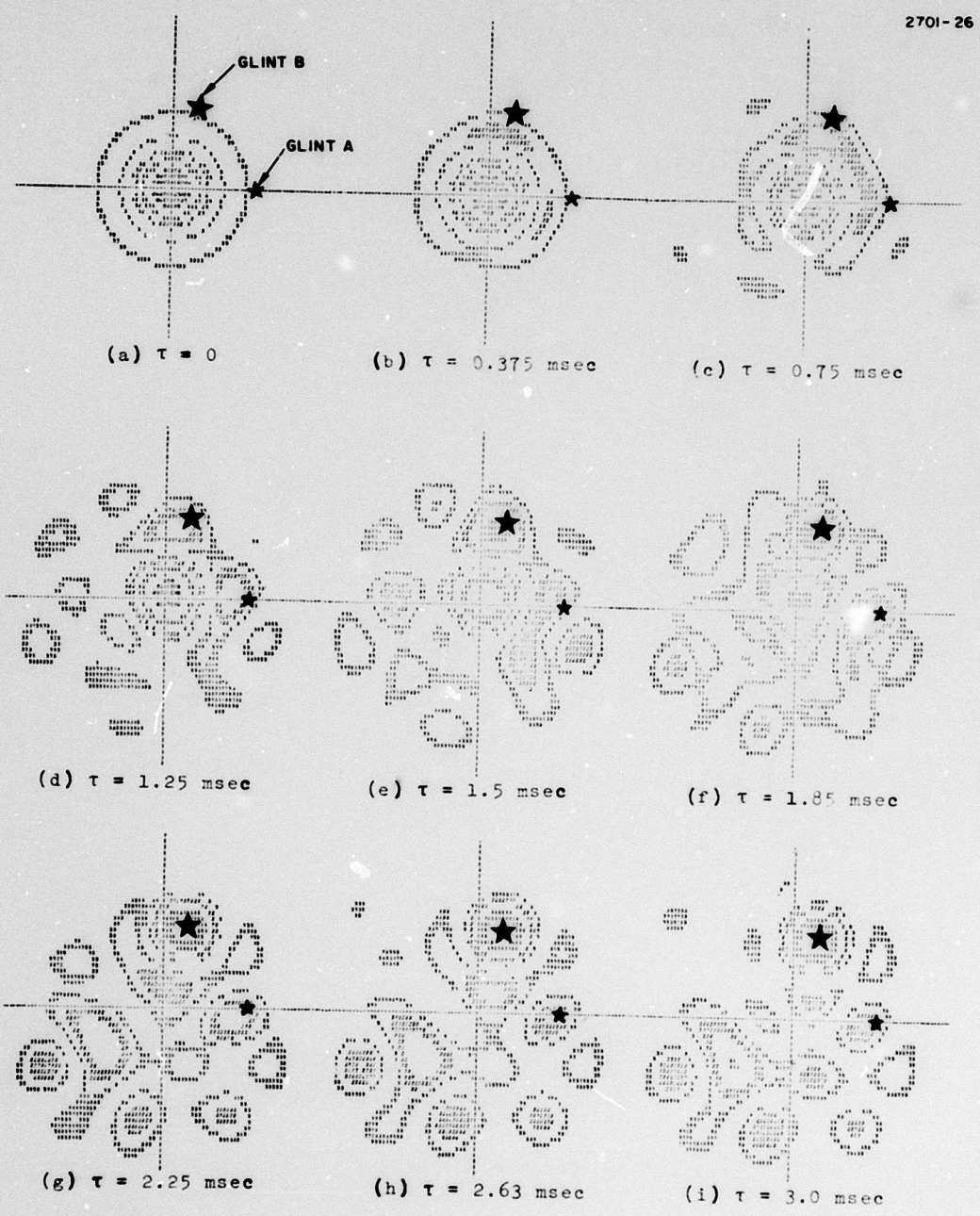

Fig. 11. Convergence sequence of 0-6-12 array for two unequal glints (glint B is 5 dB stronger) placed on the element 3 dB contour. The array is initially converged on boresight.

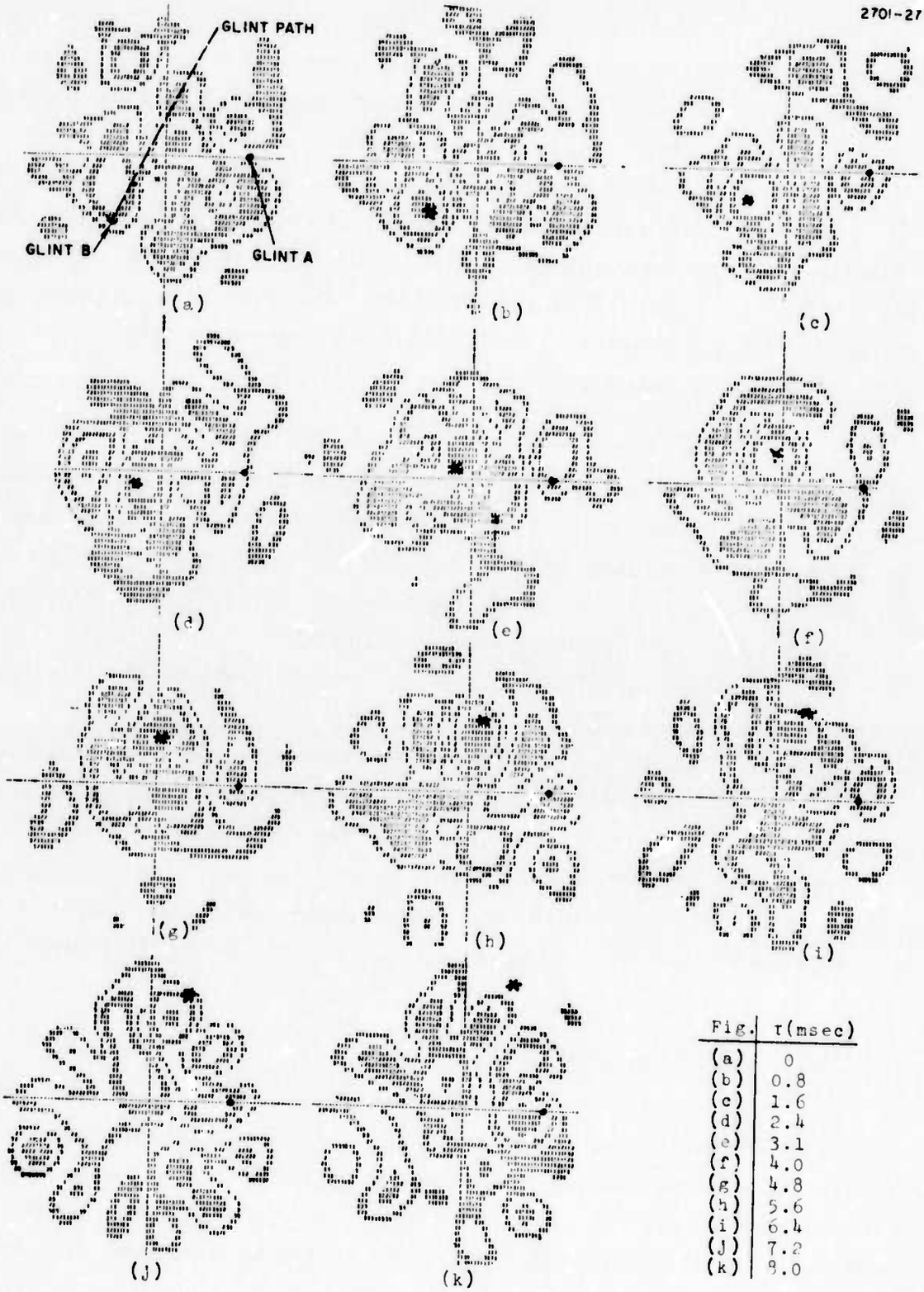

Fig.	τ(msec)
(a)	0
(b)	0.8
(c)	1.6
(d)	2.4
(e)	3.1
(f)	4.0
(g)	4.8
(h)	5.6
(i)	6.4
(J)	7.2
(k)	8.0

Fig. 12. Convergence sequence of 0-6-12 array for one moving glint (B) and one stationary glint on the element 3dB contour (A, 5 dB smaller than B). The array starts from a "random" initial phase condition.

3 dB element contour on the horizontal axis. Glint B is 5 dB larger than glint A; starts at the lower left edge of the element pattern, and proceeds across the target plane at an angular velocity of 7 mrad/sec.

The beam forms on glint B in about 1 msec (frames (b) and (c)) and tracks it as the glint moves across the target plane (frames (d) to (g)). As the moving glint nears the element 3 dB contour, the beam maximum begins to lag behind (Fig. 12(h)). The amount of lag and degree of convergence get progressively worse (frames (i) and (j)) until the system breaks lock on glint B and begins to converge on glint A (Fig. 12(k)).

4. Simulation Modifications in Progress

Two modifications to the simulation are currently being made to allow full comparison with the hardware model. The first change incorporates a five-pole low-pass filter in place of the single-pole filter with notch compensation for the phase shifter resonance. This is a relatively simple modification and no difficulty is anticipated.

The second modification will add a numerical integration over a general receiver aperture. The present computation of received power is equivalent to an integration over a very large aperture. This is analytically correct for large, unobstructed, circular receiving apertures coaxial with the transmitter aperture. The change will allow simulation of circular or annular apertures of arbitrary dimensions located anywhere in the transmit aperture plane. The hardware model has an annular aperture, where the center obscuration is due to the transmit aperture, and modifications to the shape of this aperture are planned as part of the measurements program.

5. Plans for Future Work

During the next reporting period, simulation constants will be reviewed to determine that they match design values of the hardware model as closely as possible, planning for a series of test runs will be completed, and the actual runs performed. These tests will study the convergence dynamics for target configurations similar to those which will be used on the range with the hardware system. Some of the specific aspects of the system performance to be studied are as follows:

a. The effect of AGC and limiter circuits on convergence and stability

b. The performance of "polyphase" COAT

c. The aperture phase distributions which are obtained when the system converges on a single target in a multiglint environment.

III. DESIGN AND FABRICATION

This section presents the progress of the fabrication of the COAT system hardware. The principle features of the design were detailed in the design review presented in June, 1973 and in the first quarterly report. Some improvements upon the original design have been incorporated into the hardware.

A. Phasor Matrix

The phasor matrix in a segmented optics COAT system performs the functions of (1) dividing the beam into spatially separate paths, (2) phase shifting and tagging the separate beams, and (3) beam recombination. The latest version of the phasor matrix for this system is a further refinement of the design detailed in Technical Report No. 1 of this contract. A schematic of a section of this latest design is shown in Fig. 13. The baseplates are oriented at an angle of 2.26° with respect to the input beam direction in order to compensate for beam displacement caused by refraction through the glass plates. This procedure simplifies the design of the reflective masks used for beam division. A picture of a portion of the phasor matrix is shown in Fig. 14. The phase shifters and beamsplitter plates had not been mounted when this picture was taken.

The phasor matrix is designed so that different array patterns can be used with a minimum of required alignment. The baseplates are removable with all the beamsplitter plates attached and can be accurately returned to their original positions. In this way, array patterns may be interchanged and the system realigned in about an hour. The principle realignment occurs with the phase shifters and taggers since their positions must be varied according to the particular array pattern being used.

The beamsplitter plates are oriented at Brewster's angle (56.7°) to minimize reflection losses and are made of BK-7 glass for high transmission at 4880 Å, the selected operating wavelength. They are fabricated to 5 arc-sec parallelism, 1/2-wave transmitted wavefront distortion, and have a 60/40 surface finish. The aluminized reflective patches are applied using standard photolithographic techniques. No protective overcoat is used. Each

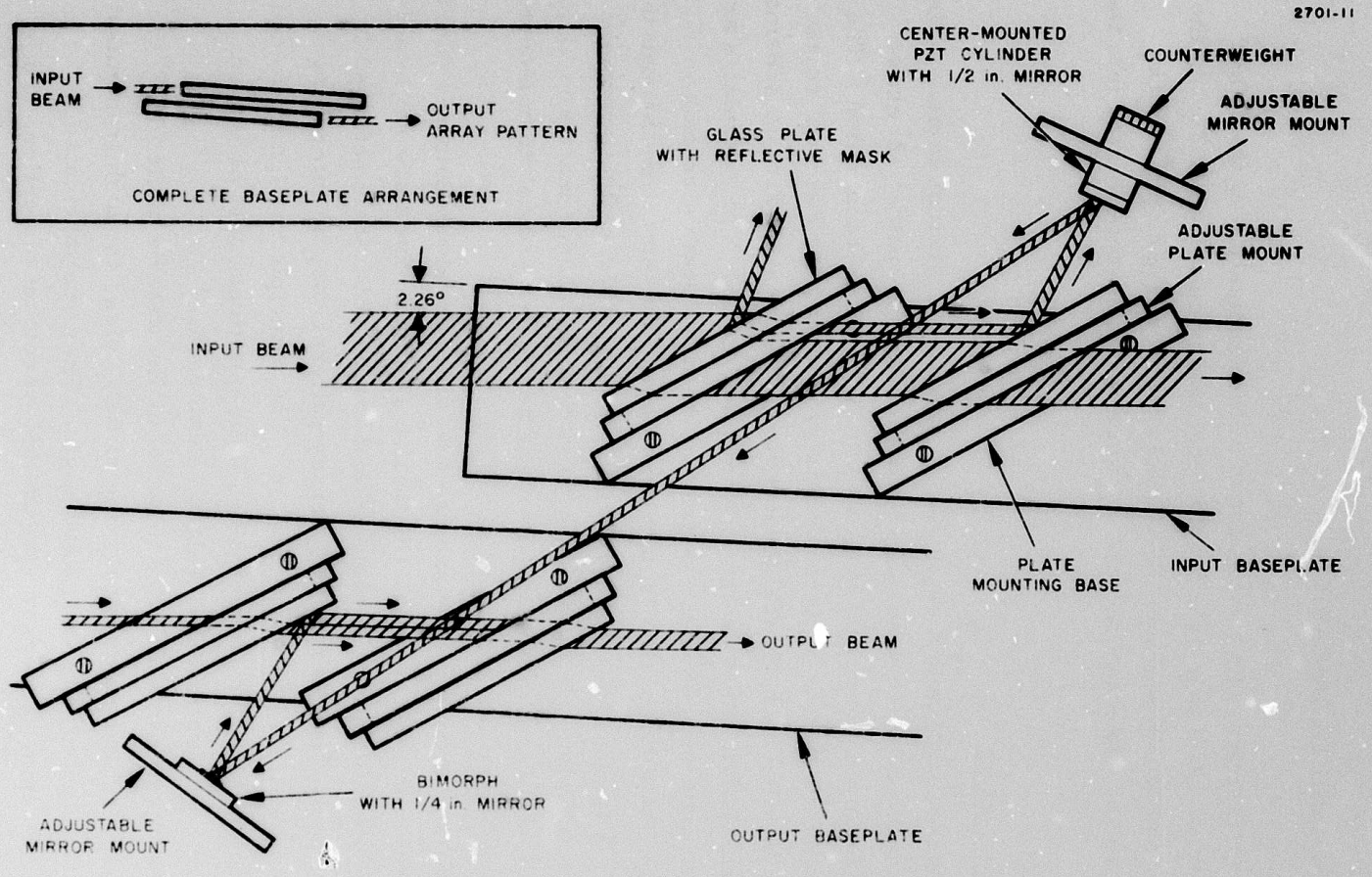

Fig. 13. Schematic of a portion of new phasor matrix design showing principle components. Inset shows the arrangement of the complete baseplate.

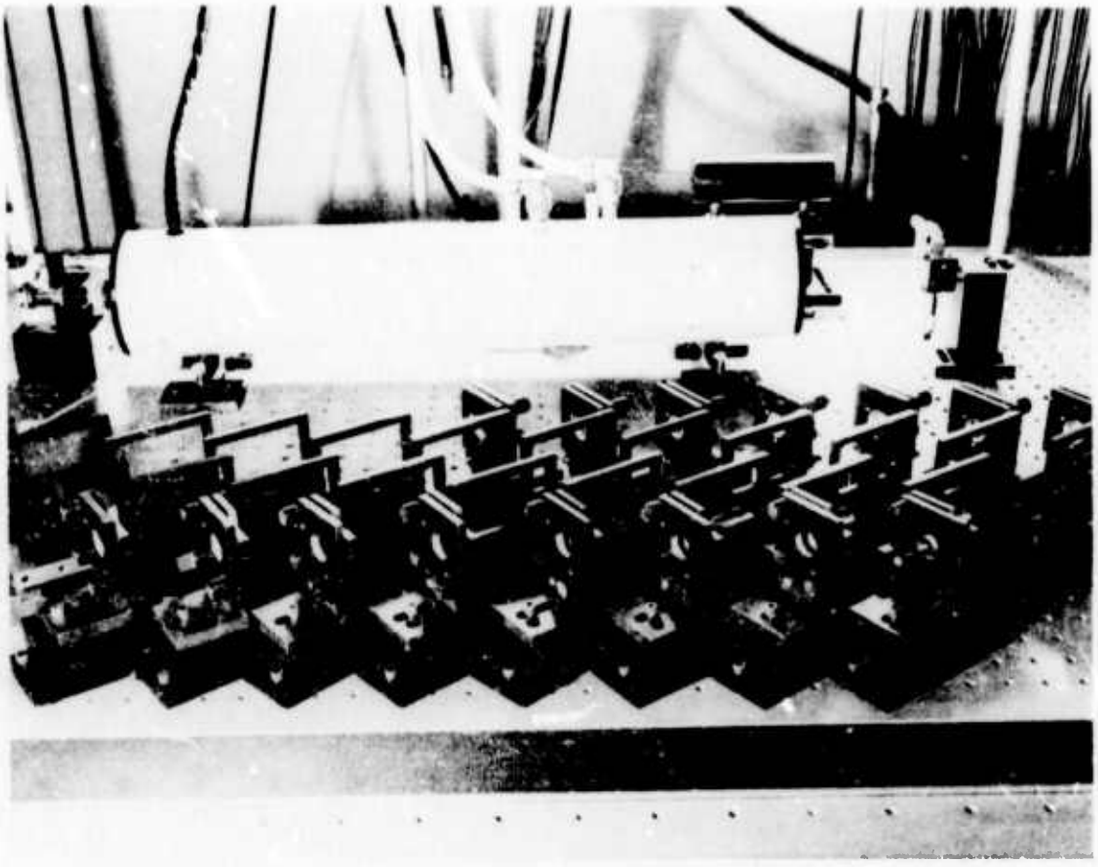

Fig. 14. Photograph of a portion of phasor matrix hardware. Beam splitter plates and PZT phase shifters are not installed.

glass plate is glued to a metal mounting plate which can be moved transversely over a small range to allow fine tuning of the relative mask alignments. When a mask is in the correct position, the mounting plate is clamped into position to hold the alignment. The assembly for the glass beamsplitter plate, the mounting plate, and the plate mounting base is shown in Fig. 15.

Figures 16 and 17 illustrate the mask layouts for the two array patterns to be studied. The rectangular patterns and crosses at the top and bottom of the masks are used for alignment. The mask patterns are offset from the center of the plates so that the center of the array pattern is aligned with the center of the clear aperture produced by the plate and its mount. The numbers on the patches indicate the order in which the sections are removed from the incident beam as it propagates through the matrix.

The 1 x 8 array will be used for initial calibration purposes since we have data from an earlier 1 x 7 COAT array. The array elements are 3 mm x 3 mm square at the phasor matrix output and thus give a continuous transmitted pattern which is 3 mm x 24 mm at the first lens of the transmitter output telescope.

The 0-6-12 array shown in Fig. 17 is the primary transmitter pattern which will be studied. At the output of the phasor matrix, each element has an area of approximately 9 mm^2 and, for convenience in mask fabrication, has a trapezoidal or modified trapezoidal shape. At the output of the phasor matrix, the annular pattern will have an inside diameter of 3.4 mm and an outside diameter of 14.8 mm. At a range of 100 meters, this array will be able to resolve glints separated by more than 4 mm. The output telescope on the transmitter can be used to increase or reduce this resolution by a factor of 2.

B. Phase Shifters and Taggers

The requirements for the phase shifters and taggers have been discussed in the first quarterly report. As discussed in that document, piezoelectric transducers were selected for both the tagging and phase-shifting functions. The specifics of the final design are discussed below.

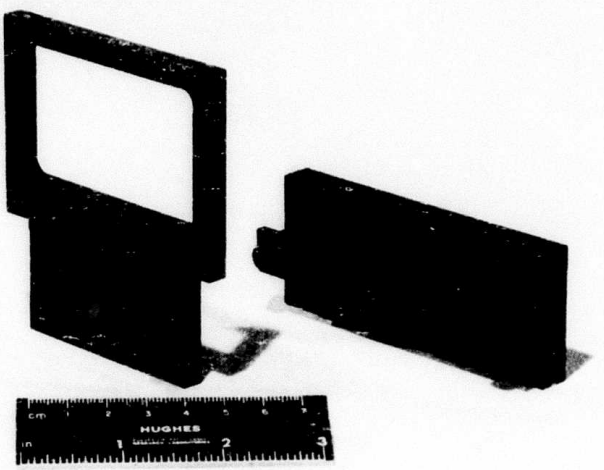

Fig. 15. Photograph of a beam splitter assembly. From left to right are BK-7 splitter plate with reflective mask, adjustable plate mount, and plate mounting base.

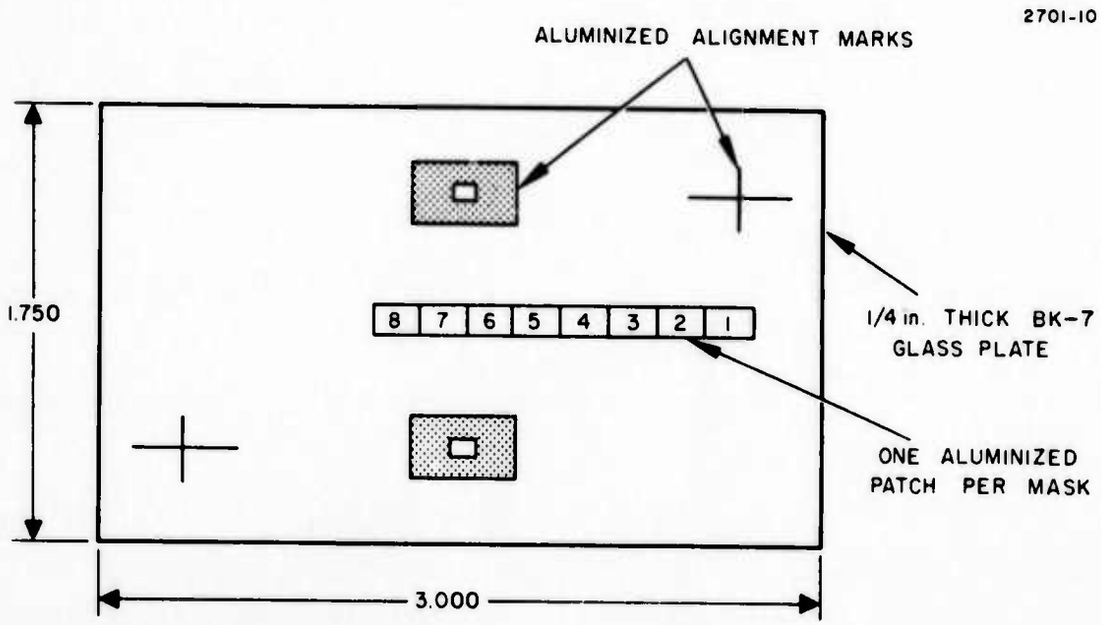

Fig. 16. Mask layout for 1 x 8 linear array. All masks have alignment marks, but only one numbered patch.

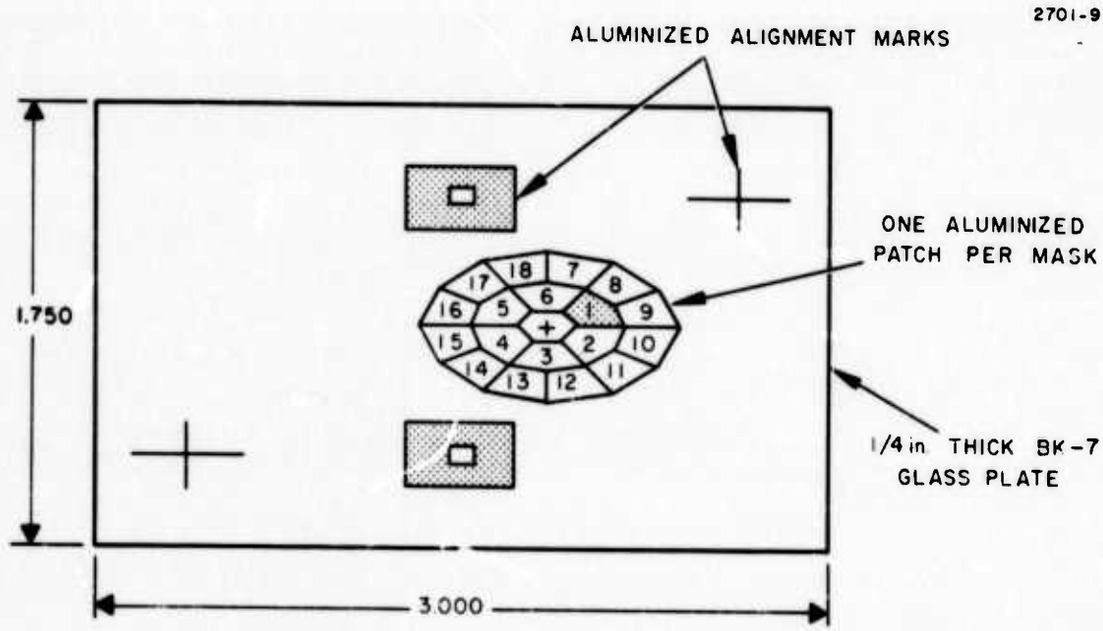

Fig. 17. Mask layout for 0-6-12 array. Numbers on array patches indicate the order of section removal from the input beam.

1. Phase Shifters

A 1/2 in. diameter by 0.021 in. thick bimorph made from PZT-5H by Vernitron Corp. was selected for use as a phase shifter. The bimorph is rigidly clamped at its perimeter and a 1/4 in. diameter x 1/8 in. thick aluminized front surface mirror is attached to its center with contact cement. This combination has a response of 125 V/μ and a 25 dB resonant peak at approximately 14 kHz. An assembly drawing for one of the 18 units is shown in Fig. 18.

The original phase shifter design also incorporated a notch filter to suppress the 14 kHz resonant peak. This notch filter has been eliminated in favor of a multistage low-pass filter. The performance of this new system has been very good as indicated by the computer simulation results. The details of the electronics design have been outlined in the analysis section and will be further discussed in a later section.

2. Taggers

A 1 in. long, 1/2 in. O.D., 1/16 in. wall cylinder of PZT-5H is the choice for driving the tagging mirror. When center mounted in the adjustable mount with a mirror and counterweight cemented on, the unit has a 24 dB resonant peak at 50 kHz. A plot of the amplitude and phase response of one unit is shown in Fig. 19. The resonance amplitude variation begins around 25 kHz, but is not significant until 35 kHz. The phase variation also is nearly flat out to 35 kHz. The units should thus be useful at frequencies up to at least 32 kHz with a low-frequency response of 645 V/μ. Any variations in response from 25 kHz to 35 kHz can be tuned out in the driver amplifiers.

The new unit has twice the response of the 1/8 in. wall PZT-5H cylinders discussed in the first quarterly report and a slightly higher resonant frequency (50 kHz versus 40 kHz). With the newly designed driver amplifiers, the taggers can provide up to $\pm 60^{\circ}$ of dither phase modulation.

Figure 20 is a photograph of the bimorph and the PZT cylinder each mounted with mirrors in an adjustable mount which is on a spacer block. The spacer blocks match the mirror height to the phasor matrix height. Each bimorph unit also has a solenoid-driven shutter in front of it which will allow removal of any desired element(s) from the transmitted array.

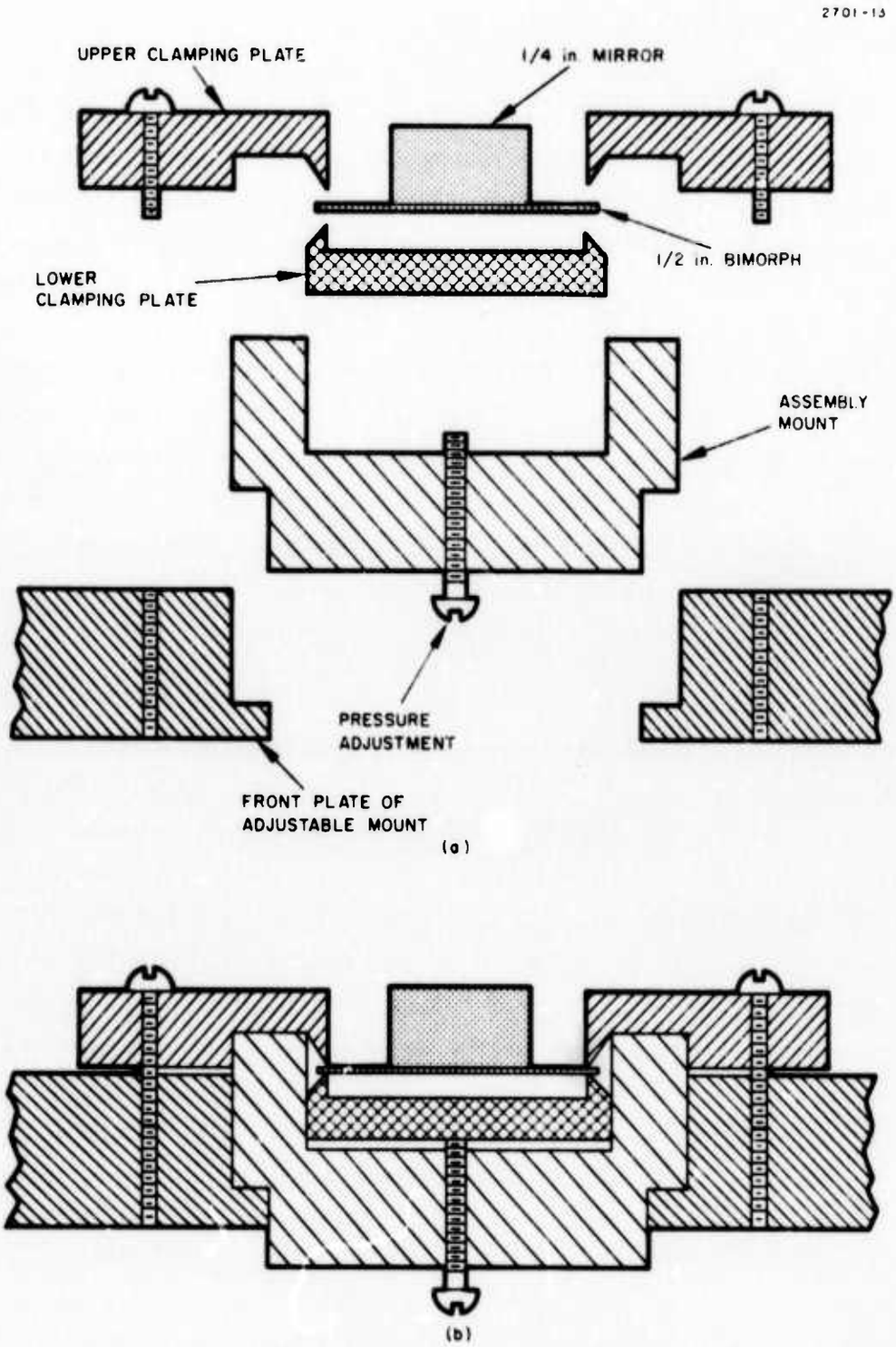

Fig. 18. Assembly drawing for 1/2 in. diameter bimorph.

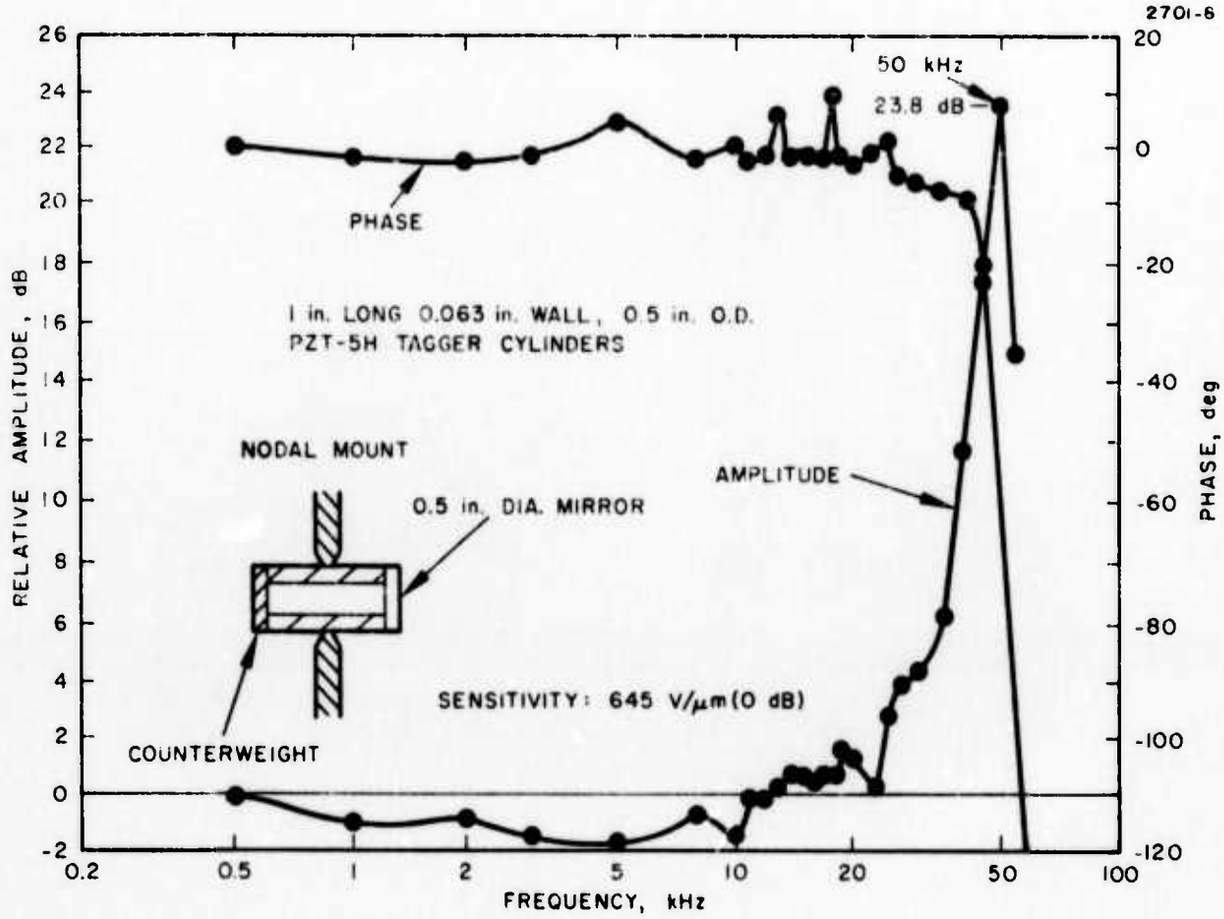

Fig. 19. Frequency response of center-mounted, 1/16 in. wall PZT cylinders with mirrors attached.

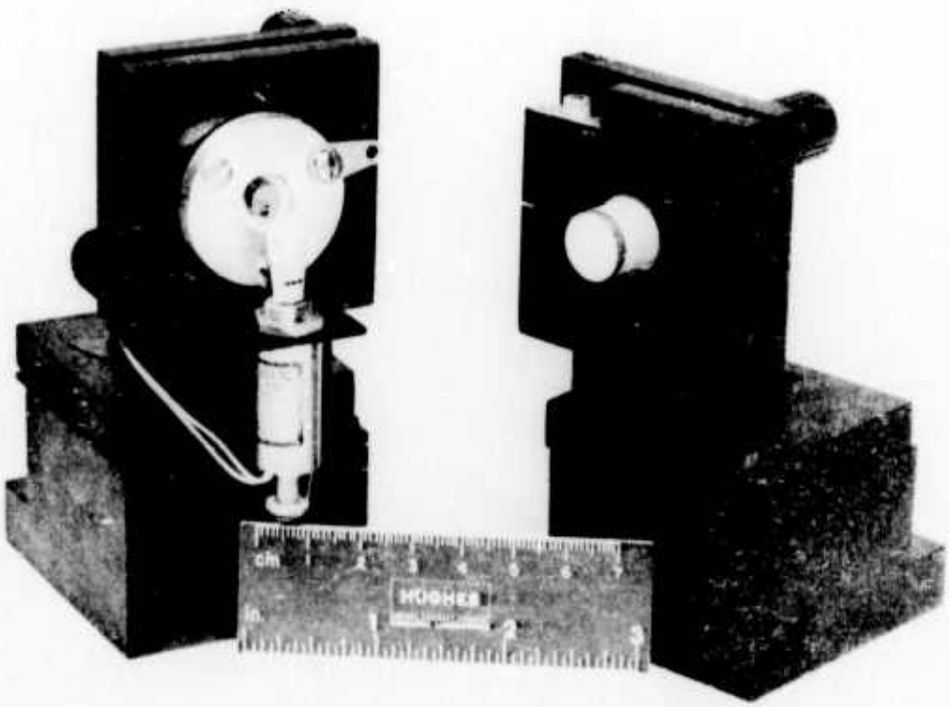

Fig. 20. Photograph of mounted phase shifters. Bimorph is on left (with solenoid-actuated shutter) and PZT tagger cylinder is shown on the right.

C. Electronic Design

A block diagram shown in Fig. 21 illustrates the main elements of the 18-element experimental COAT system. The electronics portion of this system has three elements: receiver, signal conditioning, and servo control electronics. The phasor matrix and associated phase shifters have been discussed in the two previous sections. The mechanical design of the other elements are discussed later in Sections III-D and E. The electronics separates into two main groups: a single receiver with its associated signal conditioning and the 18 channels of servo electronics. Figure 22 illustrates a further subdivision of the main element blocks into the principle subelements.

1. Receiver and Signal Conditioning

The receiver as shown in Figure 22(a) consists of a single photomultiplier tube (PMT) preceded by a narrow band optical filter and followed by a low-noise preamp. The frequency response of the preamp is limited to 50 kHz to provide a noise-limiting bandwidth. The PMT anode current is monitored by a front panel meter and by a comparator circuit which removes the dynode high voltage if a selectable maximum current is exceeded. The gain and thus the output current of the PMT can be adjusted by varying the output of the high voltage supply. A front panel BNC connector allows monitoring of the amplified and band limited video signal.

The signal conditioning system shown in Fig. 23 has three principle functions: automatic gain control (AGC), high-pass filtering, and peak limiting. As discussed in the first quarterly, the AGC system uses a chopper-stabilized design with a chopping frequency of 30 MHz. The high-pass filter is incorporated into the feedback loop of the AGC and has two stages with corner frequencies at 1 kHz. The computer simulation has shown that the system is not sensitive to the value of the high-pass cutoff frequency. The 1 kHz value is a compromise between transient "cw" rejection and minimum phase shift at the lower dither frequencies. A clipper following the AGC section suppresses transient spikes which are too fast for the AGC to remove.

As Fig. 23 illustrates, this section of the system also has some convenience features. The phase reversal control allows the system to be used in the "black hole" tracking mode and the gain control provides adjustment

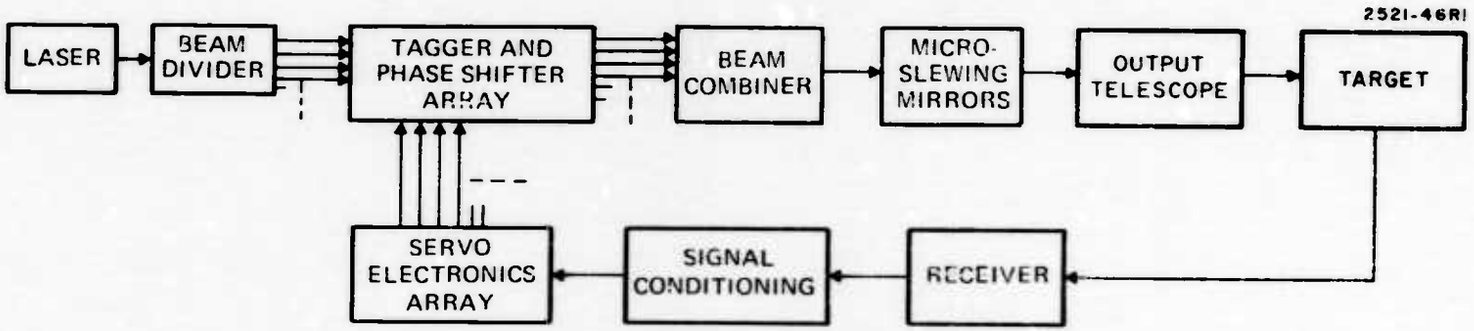

Fig. 21. 18-element system block diagram.

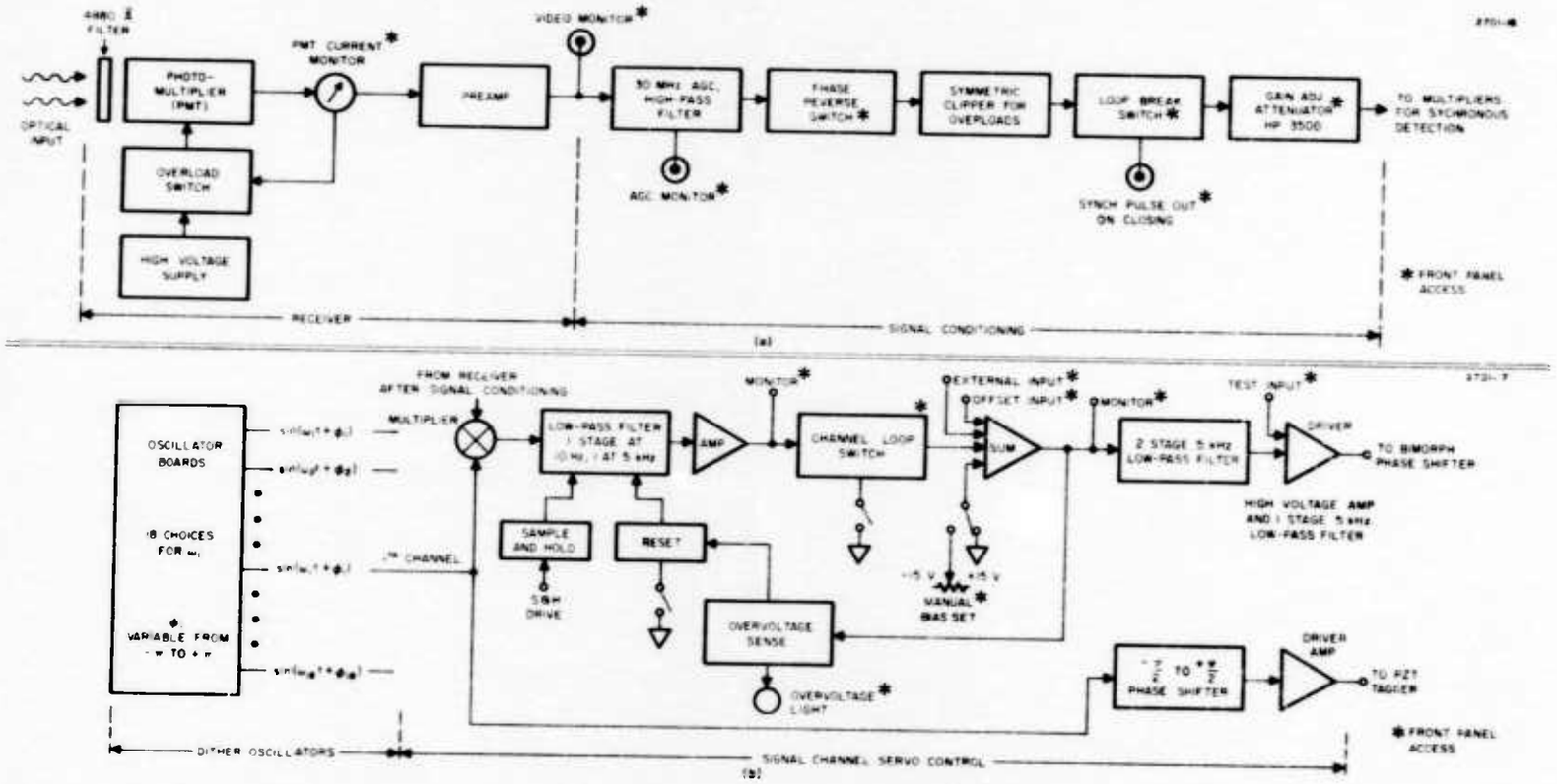

Fig. 22. COAT system block diagram. (a) Receiver and signal-conditioning. (b) Oscillator board and one of the 18 identical servo control channels.

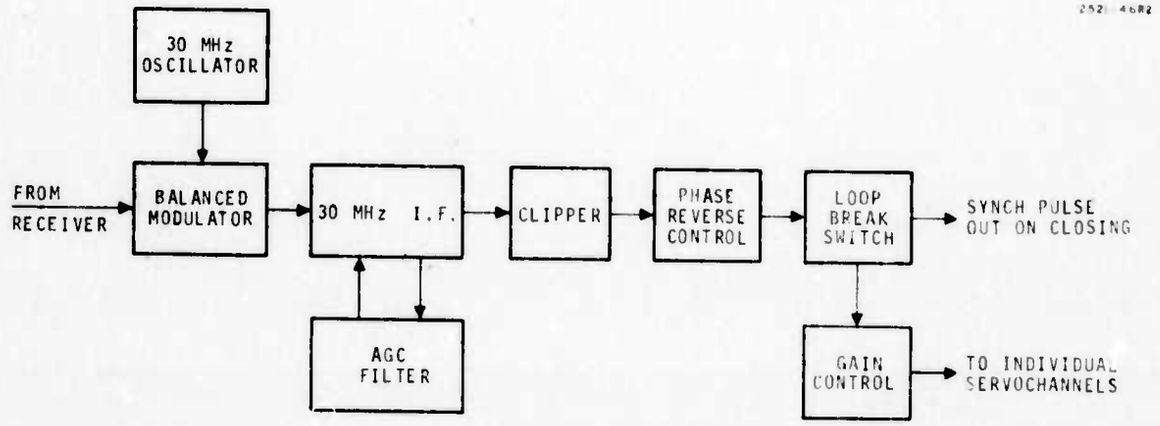

Fig. 23. Signal conditioning system using chopper-stabilized AGC.

of the small signal loop gain. This gain control is provided by a commercial 600 ohm unbalanced variable attenuator (Hewlett-Packard model 350D). There is also an FET switch for opening the loop without disabling any of the electronics. This switch closes or opens the loop in less than 10 μsec and provides a pulse output for synchronization when the switch closes. This feature will be useful when measuring convergence times for the system.

2. Servo Control Electronics

Figure 22(b) shows a block diagram of one channel of the servo control electronics. There are 18 identical channels in the entire system. Each channel has a phase shifter and driver amplifier for the PZT-driven tagger mirror. The phase shifter can be used to remove any undesirable phase shifts which might be introduced by the driver amplifier or the PZT mirror driver. It can also be used to study the effects of purposely introducing a phase shift into this part of the loop.

The phase shifter control circuitry consists of a sine-wave multiplier (Burr-Brown 4203K) for demodulating the signal from the common receiver channel, a 5-stage low-pass filter for separating the quasi-dc error signal from all of the dither frequencies and their harmonics,* a driver amplifier for the bimorph phase shifter, and sample-and-hold circuitry for use in slewing or offsetting the optical beam from the convergence point chosen by the COAT system. There is also a voltage-sensing loop which will reset the first two filter stages (10 Hz and 5 kHz corners) to zero. The reset is designed to occur before output of the driver amplifier reaches its maximum value.

The dither (tagging) oscillators are two-phase, low distortion, stable frequency devices which are constructed using two Signetics 531 ICC packages. The oscillators have been built on six boards, one board for every two channels. There are six separate oscillators and four phase shifting networks per board. The possible connections are shown in Fig. 24. This design allows the system to operate with 18 separate

*The multiplier and low-pass filter together form a synchronous detector.

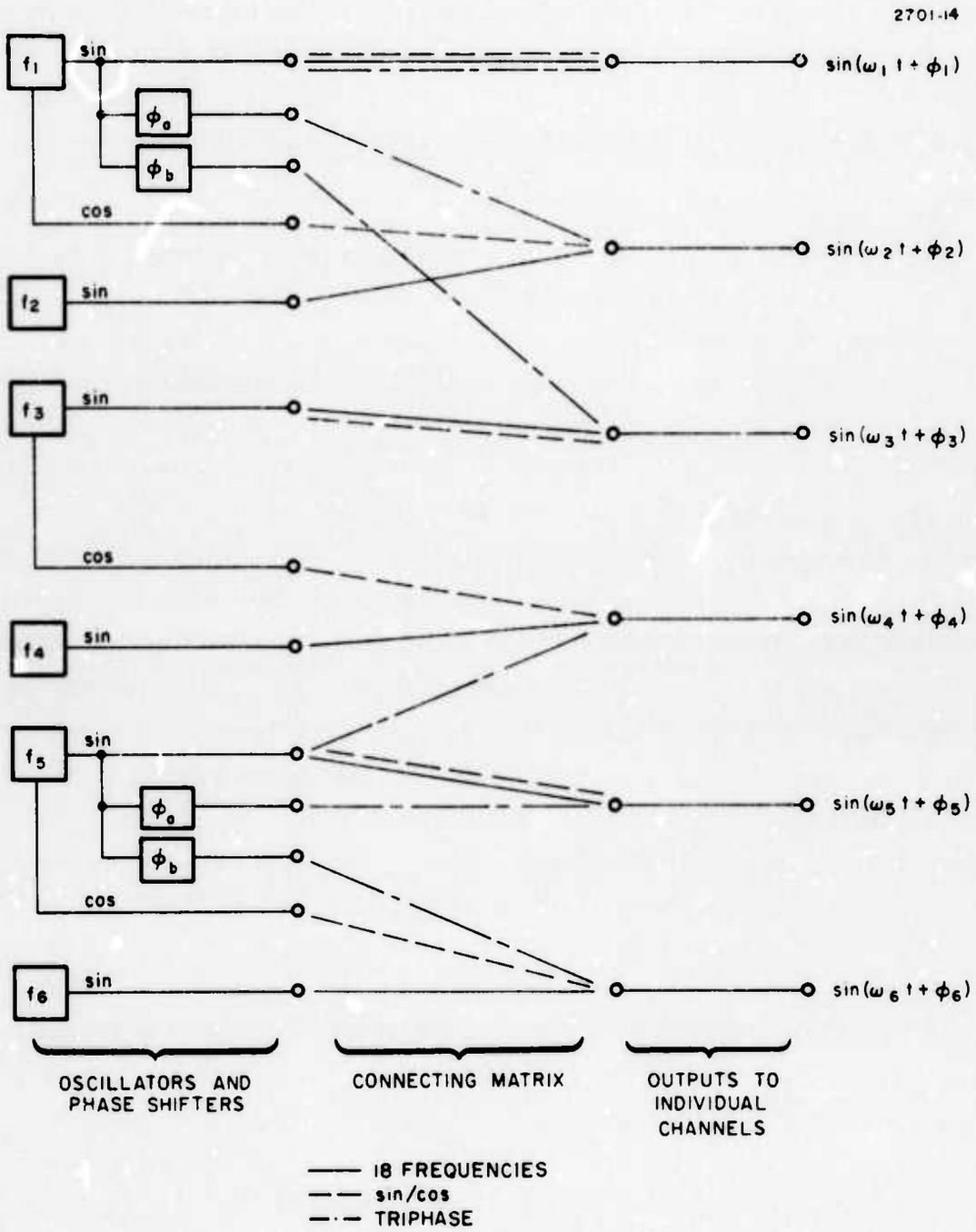

Fig. 24. Interconnection of three two-frequency oscillator boards for one frequency per channel, sine-cosine, and tri-phase operation.

frequencies, with nine frequencies so there are two channels per frequency (sine/cosine), or with only six frequencies. The latter mode is termed "triphase"* since there are three frequencies per channel and the phase shifters allow selection of arbitrary phases between the three channels. These possibilities for dither frequency configuration will enable us to check the conclusions reached with the computer simulation regarding frequencies, frequency separation, and sine/cosine and triphase operation.

The initial choice of 18 dither frequencies is shown in Table V. As discussed in an earlier section, the upper frequency limit of 32 kHz is set by the PZT tagger resonance. The lower limit should be well above the high-pass filter corner and so should be as high as possible consistent with adequate dither frequency spacing. In this case 1.4 kHz is the minimum acceptable dither spacing so that 8.2 kHz is the lowest frequency for 18 separate frequencies. Sine/cosine and triphase operation will be studied using various combinations of the frequencies shown in Table V.

TABLE V

Tagger Frequencies for 18 Channel COAT System

f_1 = 8.2 kHz	f_{10} = 20.8 kHz
f_2 = 9.6 kHz	f_{11} = 22.2 kHz
f_3 = 11.0 kHz	f_{12} = 23.6 kHz
f_4 = 12.4 kHz	f_{13} = 25.0 kHz
f_5 = 13.8 kHz	f_{14} = 26.4 kHz
f_6 = 15.2 kHz	f_{15} = 27.8 kHz
f_7 = 16.6 kHz	f_{16} = 29.2 kHz
f_8 = 18.0 kHz	f_{17} = 30.6 kHz
f_9 = 19.4 kHz	f_{18} = 32.0 kHz

T1117

*Both sine/cosine and triphase operation are special cases of the more general mode termed "polyphase". Polyphase concepts will be discussed in more detail in future reports.

The tagger driver amplifiers have been completely redesigned to drive a 0.02 μf capacitive load with up to 100 V peak-to-peak at frequencies up to 32 kHz and with no spurious phase shifts. The performance of the resulting design is shown in Fig. 25. This response was measured with 100 V p-p drive on one of the 1/16 in. wall, 1 in. long tagger PZTs. A photograph of the assembled tagger amplifier board (2 channels) is shown in Fig. 26.

As discussed earlier, the low-pass filter has been redesigned and the notch filter eliminated from the circuit. As shown in Fig. 22(b), the low-pass sections are distributed through the control channel. The single stage with a corner frequency of 10 Hz and one of the 5 kHz stages are used for the sample-and-hold (S&H) function. When the S&H drive is applied, these first two filter stages are isolated from the rest of the circuit. The holding time of the circuit will be determined by the 10 Hz filter but the recovery time after removal of the hold command is set by the overall loop response (500 Hz to 1 kHz).

The sample and hold driver circuitry has been combined with a programmable slew/offset matrix. A photograph of the front panel of the S&H electronics is shown in Fig. 27. The sample time and the hold time of the S&H driver are selected by two ten-turn potentiometers. The idea is to enable the S&H circuits, slew the beam to a chosen offset position for a selectable amount of time, and then return to the starting point for a selectable amount of time while disabling the S&H. The whole process is then repeated. In this way, maximum energy is delivered to the desired aim point and a minimum amount is put on the lock-on glint to maintain the system convergence. The time sequencing involved is shown in Fig. 28. For typical expected values of τ_{hold} = 28 msec, τ_{sample} = 2 msec, and τ_{slew} = 1.5 msec, the average power on the desired aim point will be 87.5% of the maximum available at that point.

The sample-and-hold circuitry allows adjustment of τ_{hold} and τ_{sample}. In addition, there is an adjustable bias input for each of the 18 phase shifters. This bias array can be manually set to provide electronic slewing and offset to any desired point within the element pattern of the optical array during the circuit hold time.

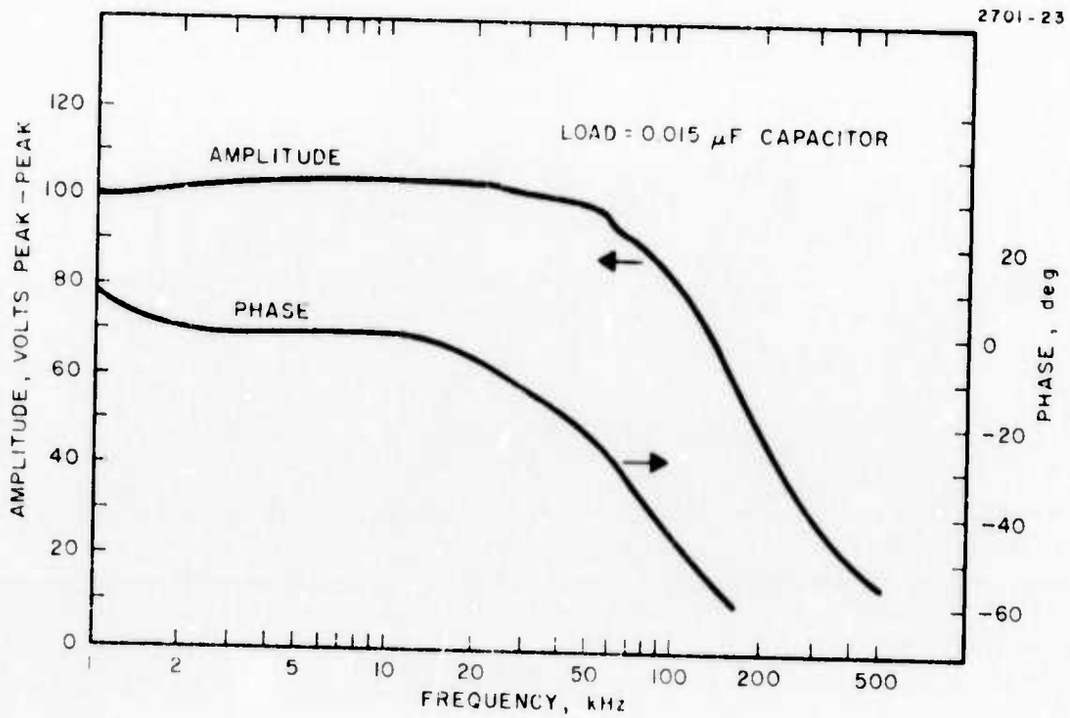

Fig. 25. Frequency response of tagger amplifier working into a pure capacitive load (same as PZT cylinders).

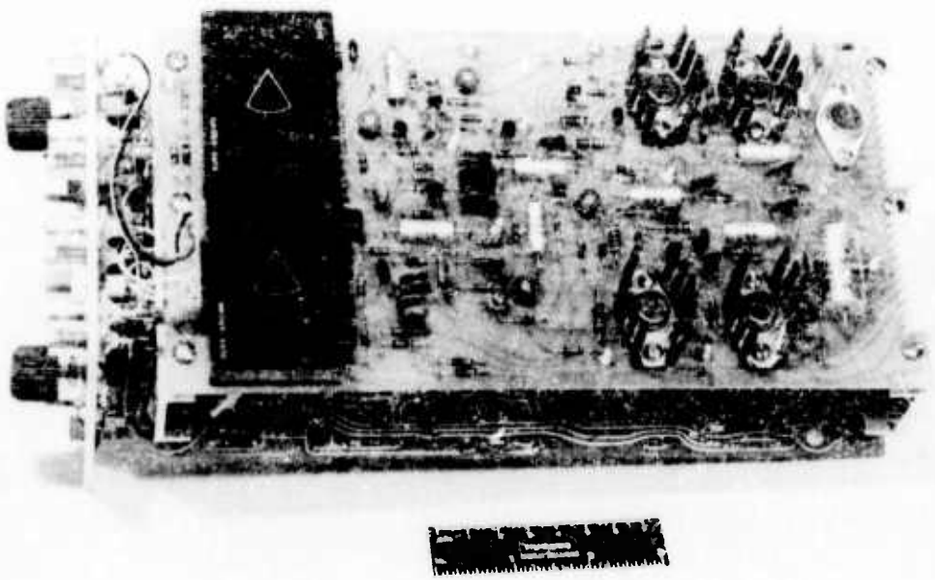

Fig. 26. Photograph of tagger amplifiers in 2-channel electronics module.

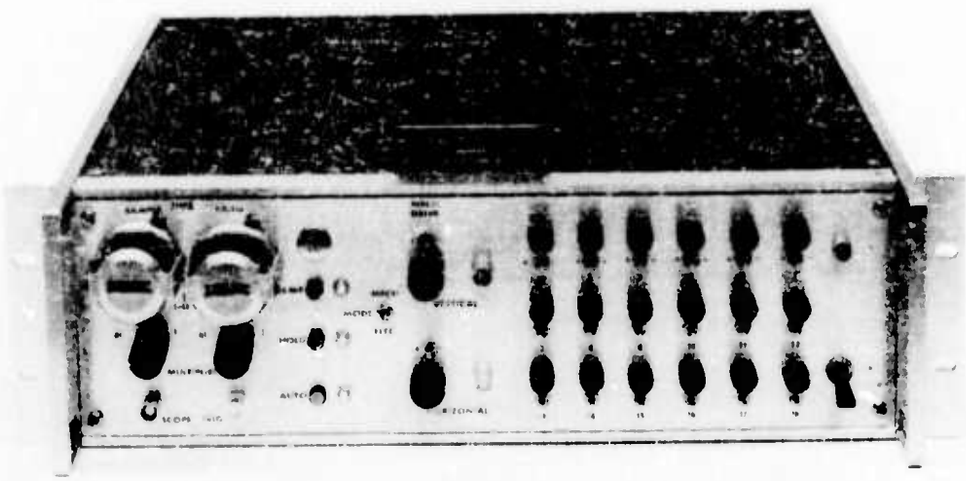

Fig. 27. Photograph of sample and hold electronics.

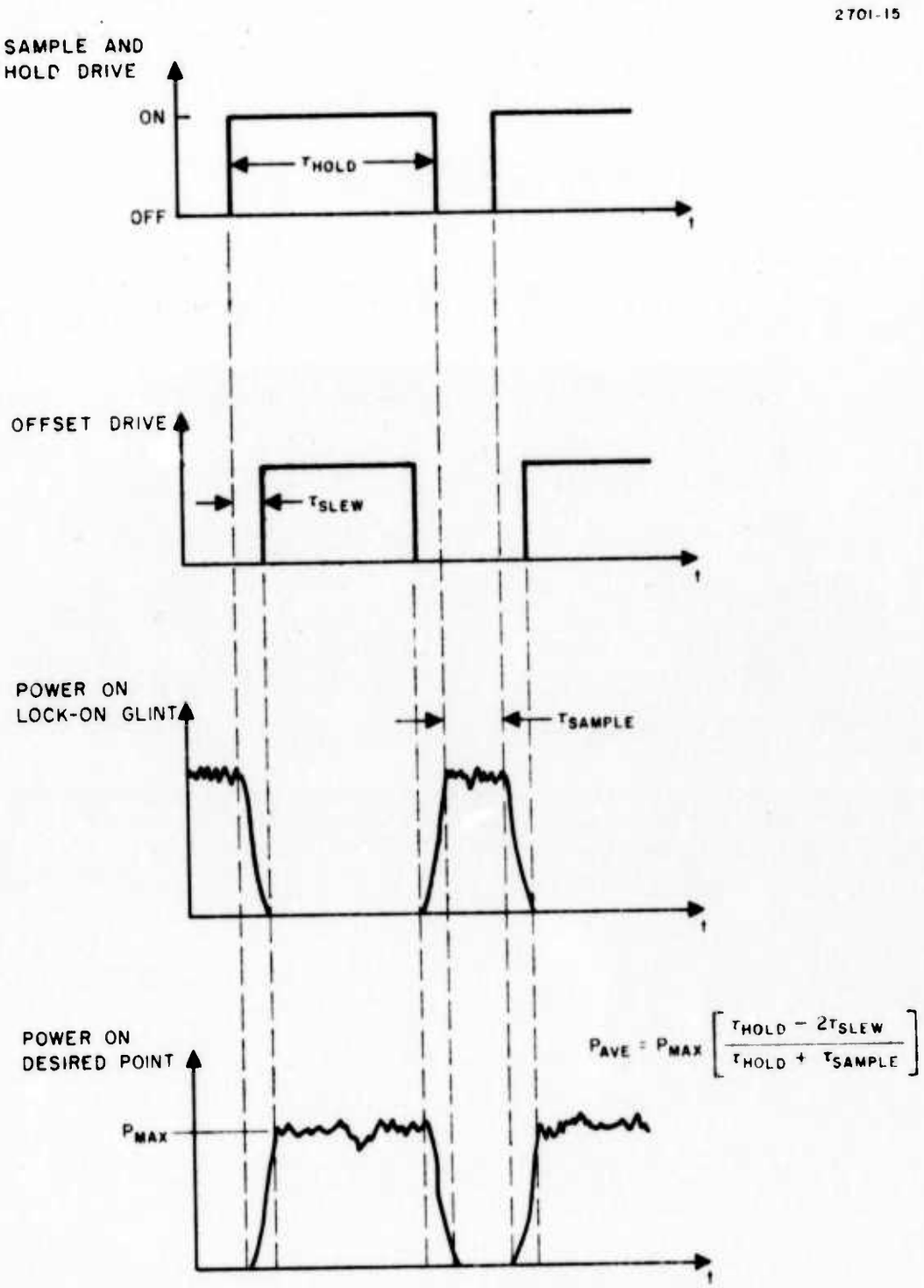

Fig. 28. Sample and hold timing sequence. The quantities τ_{sample} are independently selectable.

The system also allows a choice of electronic or mechanical slewing and offset. A switch on the S&H panel selects either the 18 programmable bias channels for electronic offset or two other adjustable voltage sources which drive a pair of microslewing mirrors, one for vertical and one for horizontal beam motion. The microslewing mirrors are located just in front of the system's output telescope. The 1-1/2 in. diameter 1/4-wave mirrors are driven by specially designed galvanometers manufactured by General Scanning, Inc. The galvanometers have up to 2° of total motion, and can slew at rates up to 1 mrad/msec for total angular excursions on the order of a milliradian. The drivers for the galvanometers are designed to provide maximum slew rate with no overshoot or ringing.

The physical layout of the servo control electronics has been designed for maximum user convenience and system flexibility. All of the controls are rack-mounted in two 6 ft high, fully enclosed cabinets. Each rack slides out on a suspension carriage to facilitate adjustments or servicing. The two racks are interconnected and are controlled from a common power switch and breaker panel. The racks also have 120 V ac convenience outlet strips mounted just inside the rear doors.

One rack holds power supplies, system on-off, and the sample-and-hold circuitry. The other unit contains the receiver electronics, AGC, and individual channel controls. There is also a digital voltmeter in one rack to provide for convenient measurement of various test points.

The channel controls are divided into 2-channel units with 3 units (6 channels) per 19 inch rack width. A photograph of the front-panel of three 2-channel control units is shown in Fig. 29. Each channel has separate controls for dither on/off, shutter open/close, loop break, manual dc bias setting, and a light to indicate when the channel is active (dither on, shutter open, loop closed). The bias is similar in function to that built into the sample-and-hold circuitry except that it is applied continuously when the bias switch is on. Each channel has an indicator light to show when the filter reset circuitry closes as well as numerous test and monitoring points; additional test points are also available on the rear of the chassis.

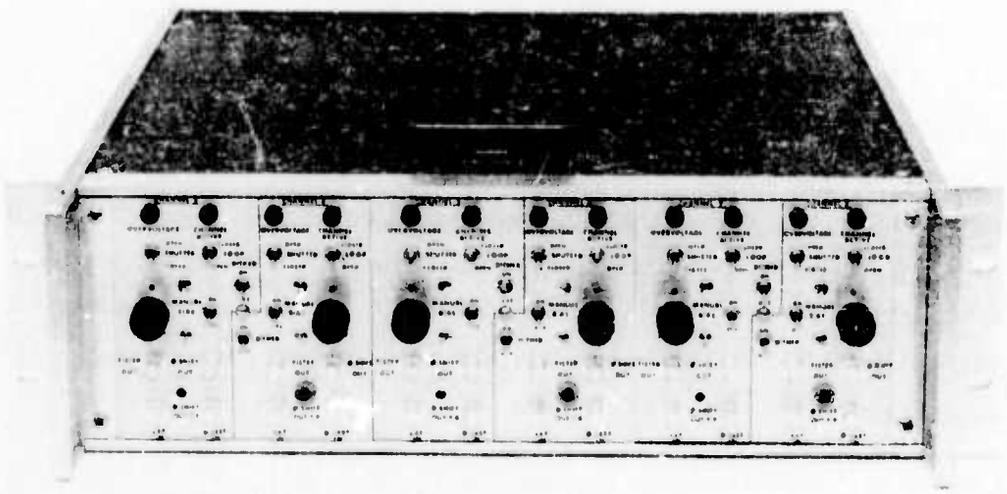

Fig. 29. Photograph of 6-channel COAT electronics panel. The 18 channel system uses three such panels.

The layout of a 2-channel board and the oscillator board is shown in Fig. 30. The system is quite compact but retains the accessibility and flexibility necessary for a research tool. The filter constants, for example, can be easily changed by changing a few resistor or capacitor values. The modular design facilitates design changes intended to optimize system operation and allows easy expansion to more channels if desired.

D. Optical Receiver

The optical receiver consists of a receiving mirror, a narrow band optical filter, a single photomultiplier tube (PMT), and appropriate masks for varying the receiver resolution and field-of-view (FOV). These elements are shown schematically in Fig. 31(a).

The receiving mirror is parabolic to within $\lambda/20$ with a diameter of 8 in. and a focal length of 48 in. The size of the collimating or exepiece lens is limited by the 3/4 in. PMT diameter. This lens is a simple plano-convex lens having a 0.5 in. clear aperture and a focal length of 3 in. These values provide a 10 mrad field of view for the receiver telescope.

The photomultiplier is an RCA 8644 3/4 in. diameter tube with an S-20 photosurface. In order to insure signal shot-noise limited operation, a narrow band (28 Å at 4880 Å) optical filter is mounted in front of the PMT. The peak transmission of this filter is approximately 58%.

The effect of the size and shape of the receiver aperture on system performance will be studied by placing opaque masks in front of the receiving mirror. Figure 31(b) illustrates one type of mask, an annular ring, which reduces both the total area and the resolution of the receiver. Other types of masks will be used to determine the effect of obscuring various portions of the receiver aperture and to verify the theoretical conclusion that the receiver aperture must be at least as large as the transmitter aperture.

There is some theoretical indication that the lock-on stability of a COAT system in a multiglint environment will be enhanced if its FOV is restricted after the system converges on the strongest glint. With a restricted FOV, the appearance of stronger glints within the unrestricted receiver FOV should have little effect on the convergence state of the system.

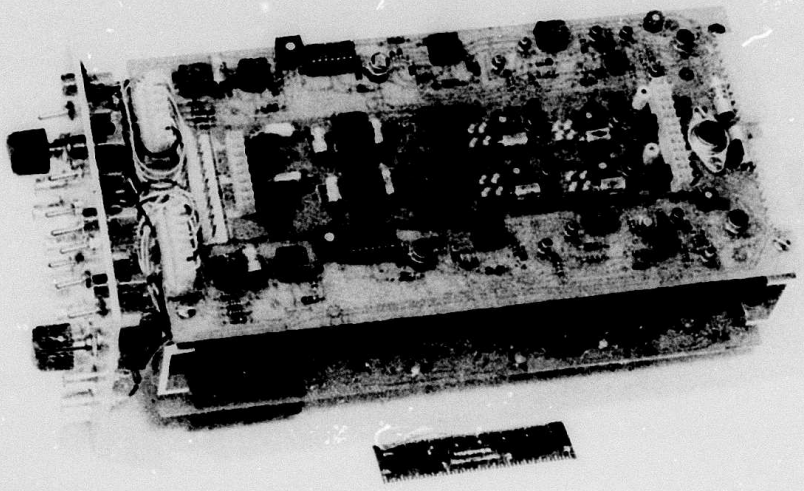

(a)

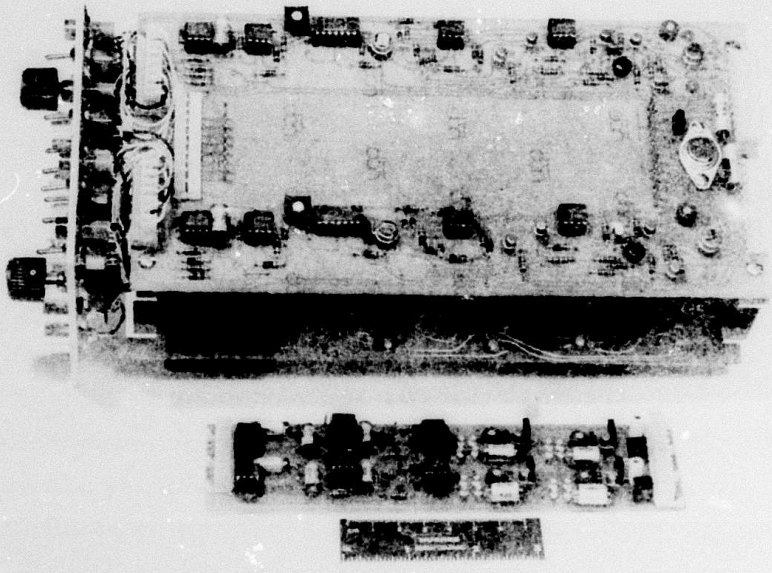

(b)

Fig. 30. Photographs of control loop circuitry for a 2-channel module. (a) With 6-frequency oscillator board in place. (b) With oscillator board removed.

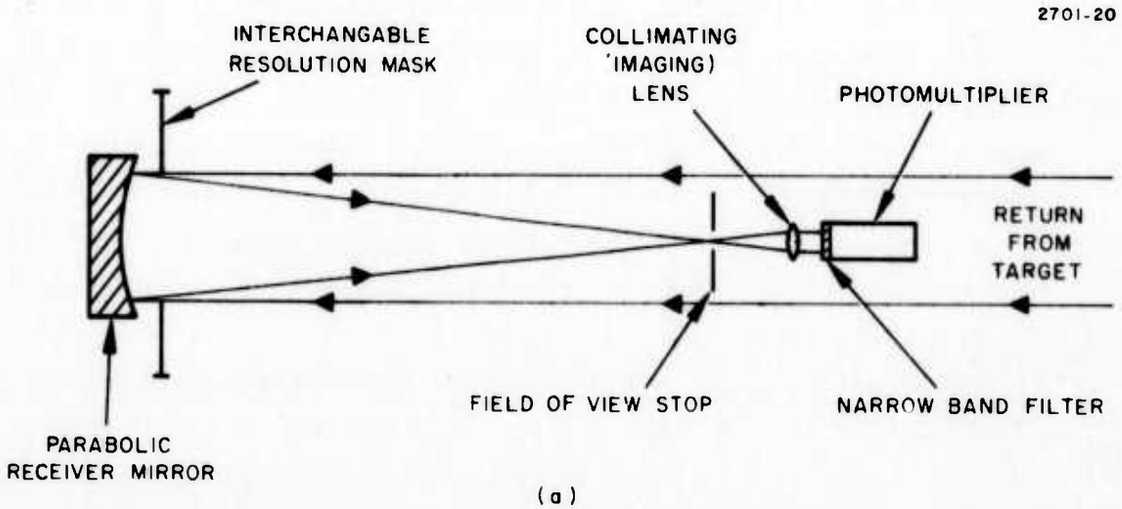

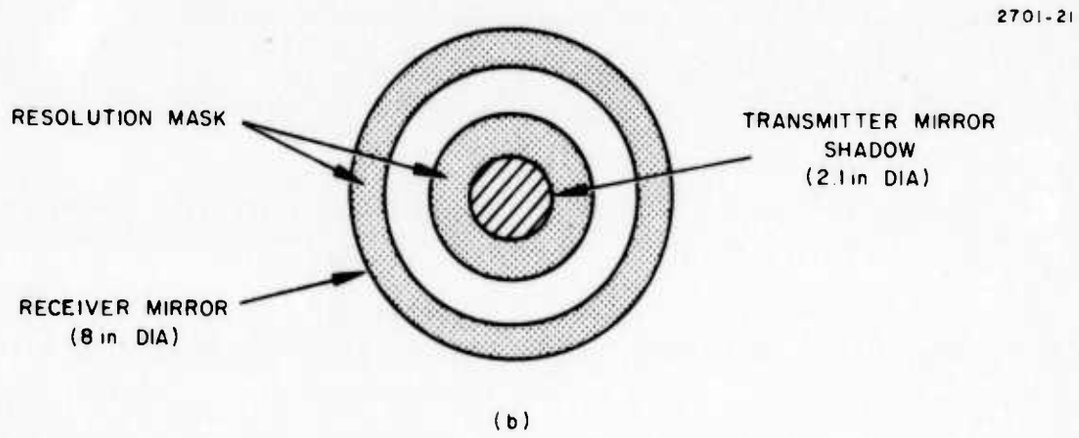

Fig. 31. Schematic of COAT optical receiver. (a) Complete receiver. (b) Example of a mask restricting receiver resolution.

This hypothesis will be checked by positioning pinholes of various sizes in the focal plane of the primary mirror as indicated in Fig. 29(a).

E. Overall System Configuration

The mechanical layout of the system has been designed for maximum convenience and flexibility. A schematic of the system is shown in Fig. 32. The 3 ft x 8 ft honeycomb-core breadboard made by the Newport Research Corporation provides a flat, rigid base which is still light enough to be moved without excessive difficulty. The breadboard also has 1/4-20 tapped holes on 1 in. centers to facilitate mounting of all the various components. With the exception of the electronics, the entire COAT transmitter/receiver is contained on this breadboard.

All flat optical surfaces in the main beam path are flat to within a quarter wavelength; the 9% beamsplitter and the output mirror are flat to better than 1/10 wave. The output telescope uses large aperture, non-diffraction-limited lenses, but careful alignment, monochromatic light, and the use of only a small portion of the total lens aperture will provide nearly diffraction-limited performance. Any residual imperfections in the output optics should be corrected out by the COAT system itself, but every effort has been made to minimize distortions in the optics. In this way, phase errors across the COAT transmitter aperture will be primarily in response to atmospheric or target variations.

As shown in Fig. 32, a half-wave plate is used at the output of the argon laser to rotate the plane of polarization so it is horizontal. The beam is then sent through a spatial filter comprised of a 10x microscope objective and a 15μ pinhole. The clean gaussian beam is recollimated to either 20 or 30 times its original diameter by use of a 330 mm or 508 mm focal length lens. The gaussian beam thus can have a $1/e^2$ intensity diameter of 2.5 cm or 3.75 cm. This allows adjustment of the uniformity of the beam intensity over the array pattern although there is a tradeoff between element-to-element power uniformity and total array output power.

Each element in the optical path is mounted with sufficient degrees of freedom to facilitate precision alignment. The mounts in conjunction with the baseplate also provide adequate rigidity and stability so that the system

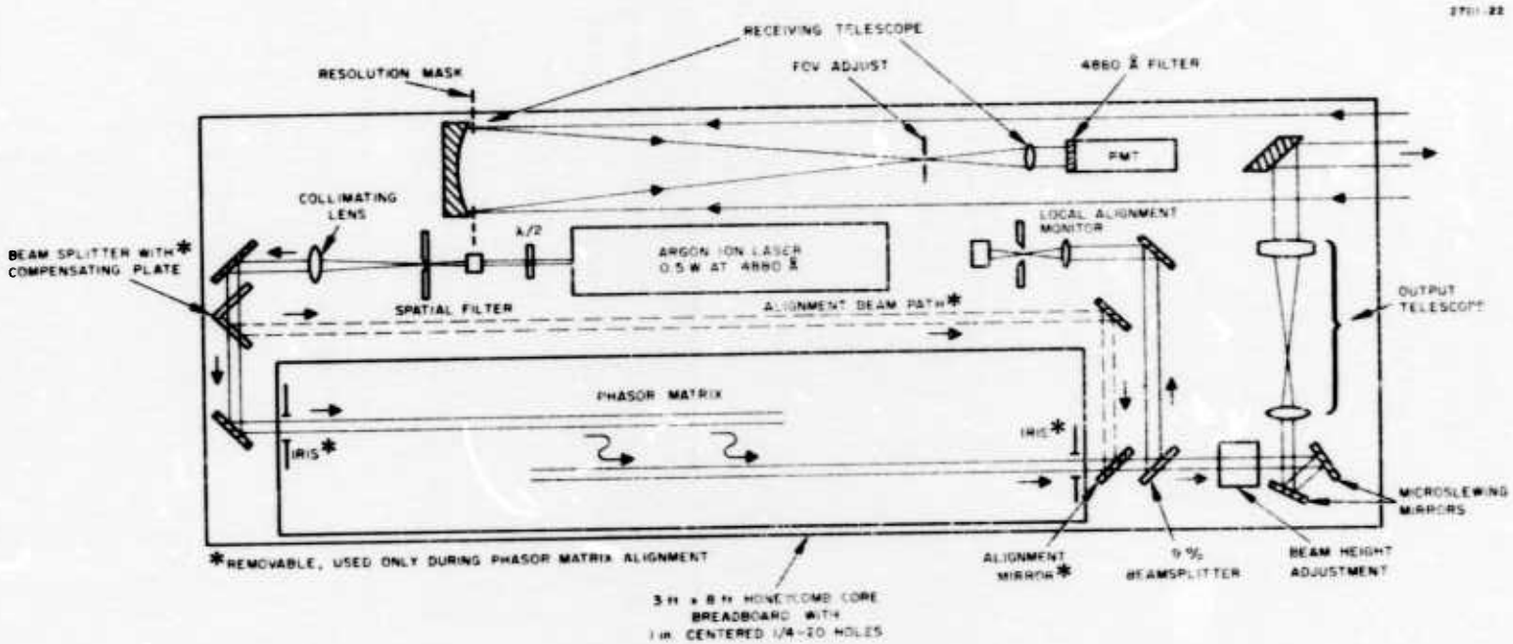

Fig. 32. Schematic of complete COAT transmitter/receiver layout.

should maintain its alignment for long periods of time. A local monitor of the alignment state is included in the system to provide a quick and continuous check on the alignment of the phasor matrix. This monitor has a silicon photodiode behind a 15 micron pinhole which is located in the focal plane of a 10 cm focal length lens.

The phasor matrix is the most difficult element of the system to align. To facilitate alignment, an auxiliary alignment beam is provided by the removable 50% beamsplitter shown in Fig. 32. The beamsplitter is mounted with a compensating plate so that the beam directed to the entrance of the phasor matrix remains undeviated when the beamsplitter is put in place. The auxiliary beam is directed to the output side of the phasor matrix by a removable alignment mirror. By initially aligning the input and auxiliary beams so they are exactly antiparallel, the phasor matrix can be completely aligned in about an hour. Both the beamsplitter and the alignment mirror are on kinematic mounts so they can be removed and replaced with no change in alignment.

The final transmitter/array optical parameters are shown in Table VI and a photograph of the transmitter/receiver is shown in Fig. 33. The electronics connections and the microslewing mirrors were not in place when the picture was taken. As can be seen, the system is compact and self-contained to facilitate transport and realignment for field tests.

F. Target

1. Glint Design

Several "cat's eye" glints have been constructed using two slightly different designs. The first design is a refinement of the glint described in the previous report. A schematic and a photograph of this glint is shown in Fig. 34. The input/output aperture is 4 mm and the lens is chosen to provide an F-number for the glint of 27. A straightforward calculation shows that in the far-field of the glint aperture, the glint reflectance varies as

$$\frac{R(d)}{R(0)} = \frac{1}{\left(1 + \frac{d}{\lambda F^2}\right)^2} \qquad \text{(III-1)}$$

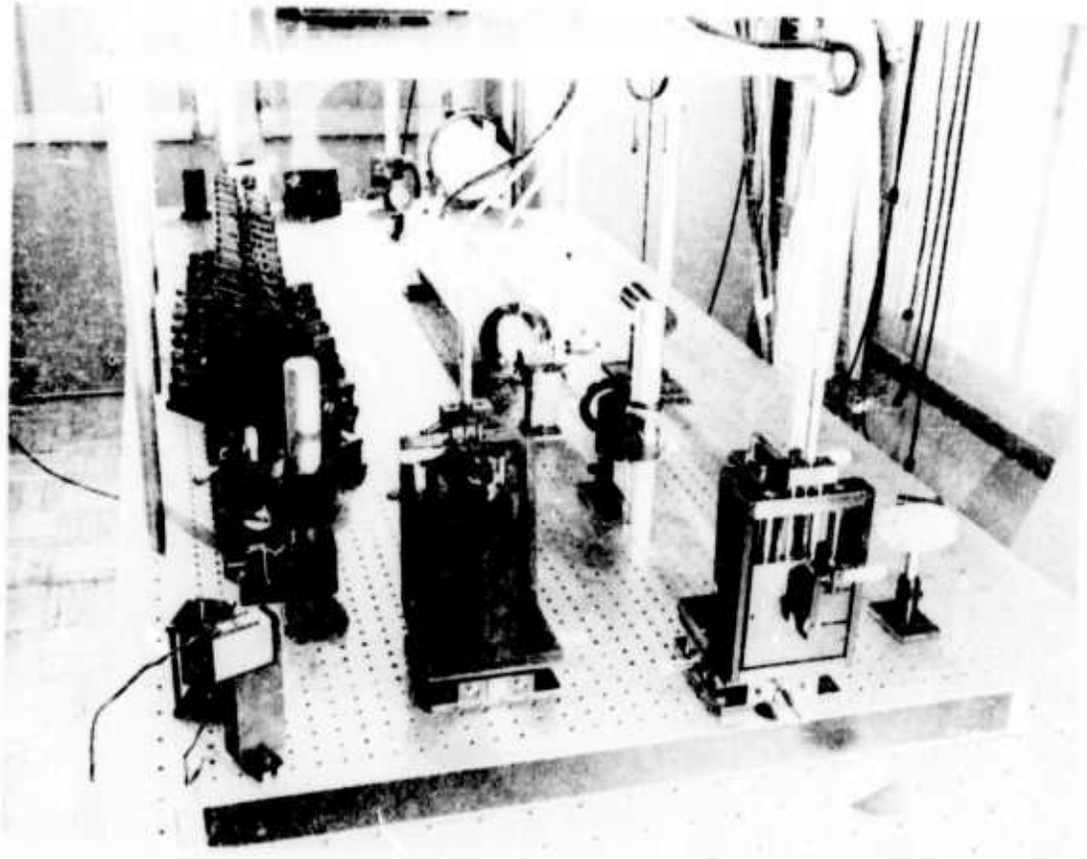

Fig. 33. Photograph of COAT transmitter/receiver.

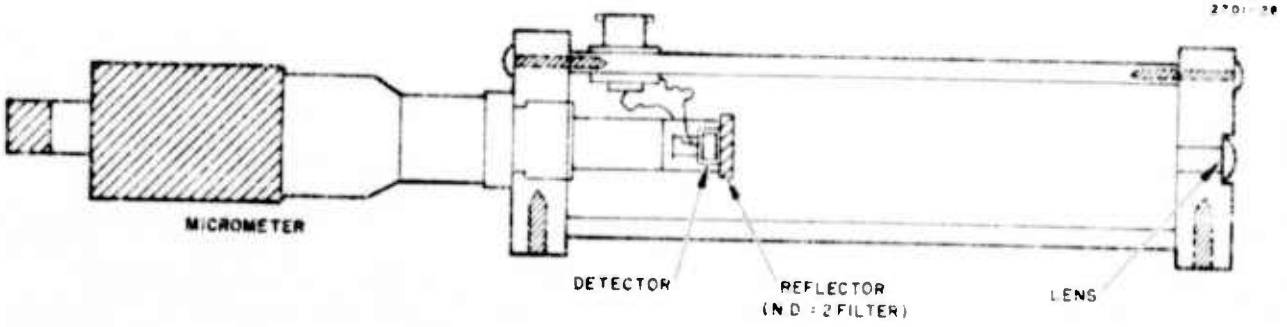

(a)

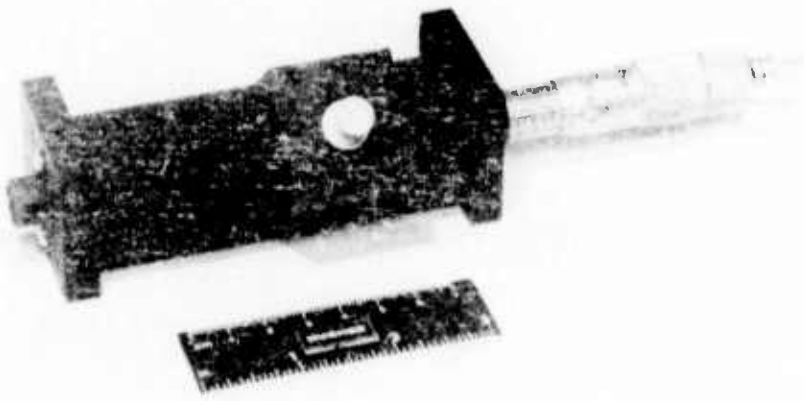

(b)

Fig. 34. Cat's-eye glint, first design. (a) Schematic. (b) Photograph of assembled unit.

TABLE VI

COAT System Optical Parameters

Transmitter	
Operating Wavelength	4880 Å
Maximum phasor matrix illumination power	0.5 W
Phasor matrix output power	Variable with array and element-element power uniformity desired
Phasor Matrix Array Patterns and Sizes (system capable of others)	1 x 8: 3 mm x 24 mm 0-6-12: 2 annular rings, dark core 3.38 mm I.D., 14.76 mm O.D.
Output Telescope	1/2x, 1x, or 2x phasor matrix output
Maximum Beam Diameter at System Output	2.0 in.
Beam Slewing Method	Selectable: electronic or mechanical
Receiver	
Receiving Mirror	8 in. diameter, f/6 parabolic, central 2.1 in. obscured
Receiver resolution	Variable using mirror masks
Receiver Field of View	Variable using pinholes at mirror focal plane
Detector	Single photomultiplier with S-20 surface preceeded by 4880 Å filter

where F is the glint F-number, λ is the light wavelength, d is the distance of the reflecting surface from the lens focal plane and R(0) is the reflectance at d = 0. Equation (III-1) shows that for our glint design a factor of 10 change in reflectance can be obtained by changing d only 0.77 mm.

This glint design uses a N. D. = 2.0 reflective neutral density filter as the reflector. This surface is mounted in front of a silicon photodetector normal to the common micrometer and lens axis. As indicated in the previous quarterly report, the directivity pattern of this type of reflector in a cat's eye glint is sensitive to alignment, but careful construction and use of a large F-number should minimize any difficulties. A 5 mm x 5 mm aperture turning prism can be mounted on the front of the glint so that several glints can be placed in close proximity; the incident beam then arrives normal to the internal axis of the glints.

The second type of glint is shown in Fig. 35. It differs from the glint of Fig. 34 mainly in the placement of the detector; the same F = 27 optics are used. A 10% reflective surface is mounted to direct part of the incident light to a silicon photodetector while passing most of the light onto a second surface which acts as the reflector for the glint. The beamsplitter is mounted at a small angle so that the glint reflectance as well as the power sampler calibration is fairly insensitive to the input light polarization. The advantage of this design is that either a diffuse or a reflective surface can be used; The glint reflectivity pattern is less sensitive to the alignment of a diffuse reflecting surface. A completed module of this second design is shown in Fig. 35(b).

2. Glint Positioning Mechanism

Three glint modules will be mounted on a 9 in. diameter plate as shown in Fig. 36. Each glint module has an independent clamping arrangement which provides positioning in both the radial and angular directions. This positioner is now under construction on a schedule consistent with the transmitter/receiver completion date.

3. Target Assembly and Glint Motion

The various glints and the glint positioning mechanism is mounted with a spacer to a reinforced 19 in. wide rack-mount panel. This

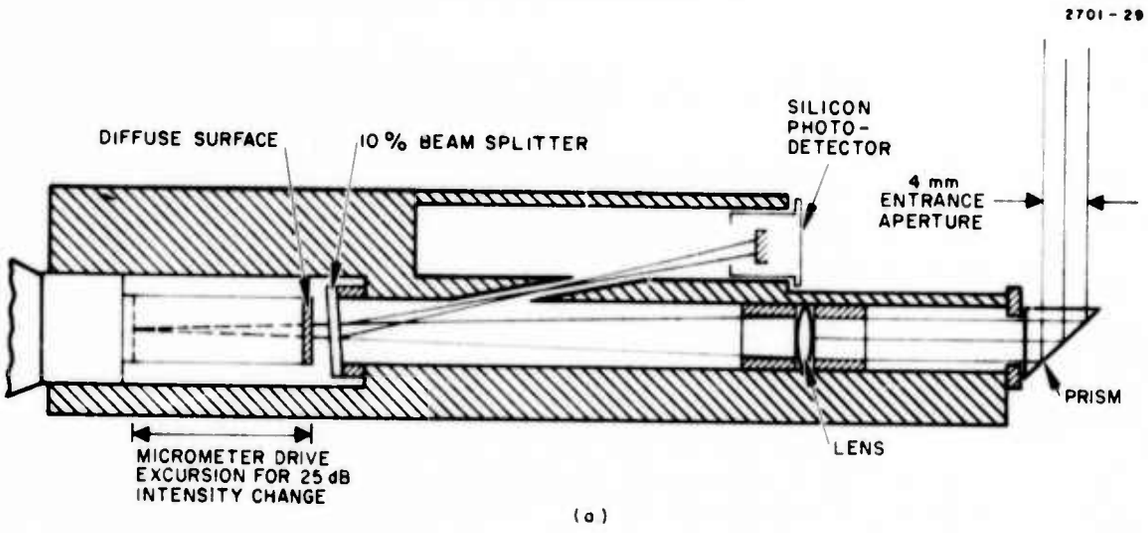

(a)

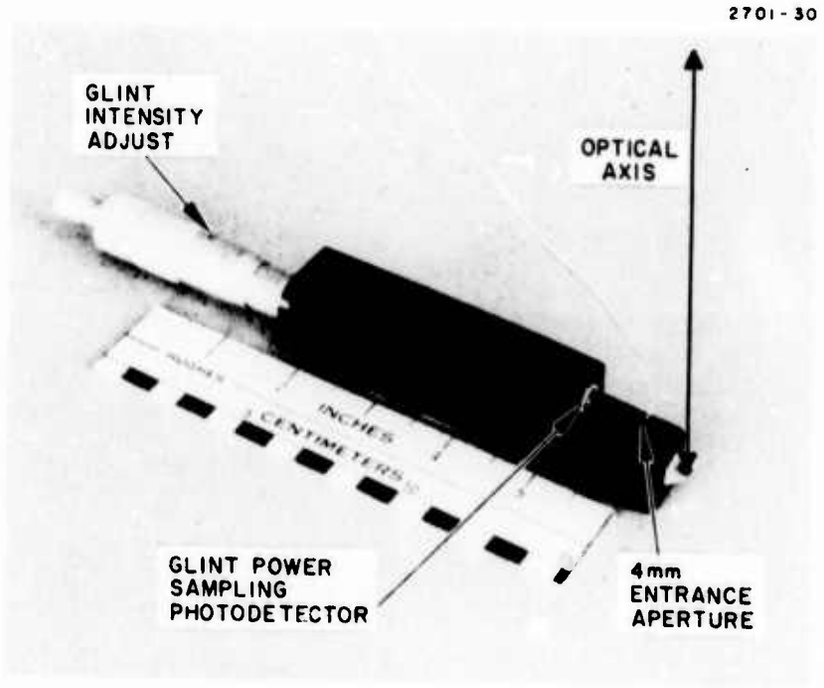

(b)

Fig. 35. Cat's-eye glint, second design. (a) Schematic. (b) Photograph. Reflecting surface is changeable in this design.

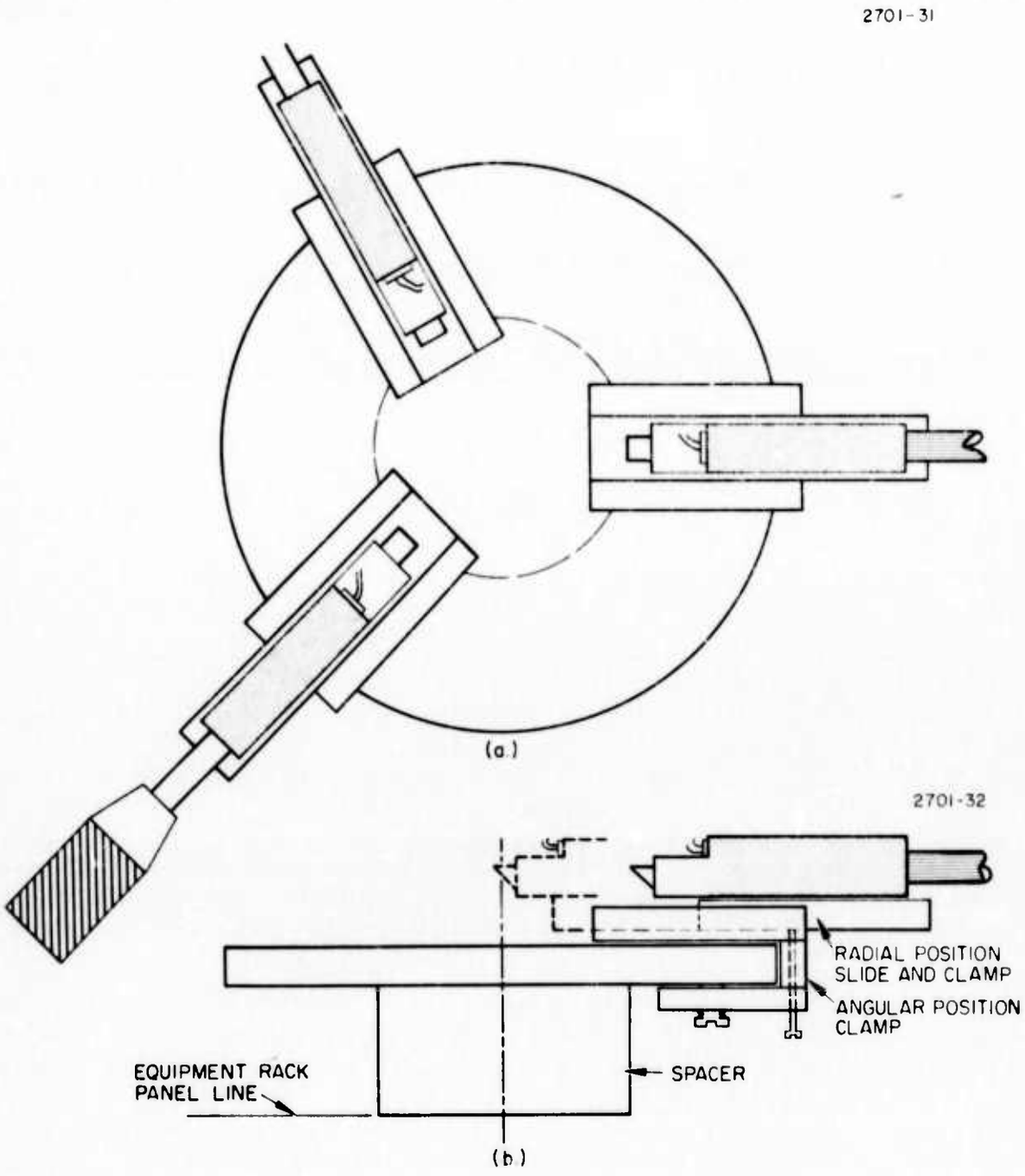

Fig. 36. Glint positioning mechanism showing three glint modules. (a) As seen by transmitter. (b) Side view showing how modules are moved.

panel is mounted in a standard vertical rack which also contains all the beam and target monitoring instrumentation. A schematic of the rack layout is shown in Fig. 37.

For static glint tests, the incident beam will fall directly on the target except for a beamsplitter arrangement used to monitor both the incident beam profile and the target configuration. A schematic of the arrangement is shown in Fig. 38. For static tests, the input beam has position B_1.

For moving glint tests, the beam comes in at B_2, turning mirrors M_1 and M'_1 are put in place, and a scanning mirror M_1 is added. The adjustable glints are arranged so that those in the receiver field of view through M'_1 appear stationary and those seen through M_1 appear to move. Mirrors M_1 - M_4 all mount on the same panel as the glint positioner.

The scanning mirror will be capable of moving $\pm 3^{\circ}$ at rates up to 3 Hz along two orthogonal axes. This motion will provide target motion rates up to 10 mrad/sec as viewed by the COAT transmitter and receiver. Independent drive control for the two orthogonal axes is desirable, but not essential for the tests to be performed on this contract. Consequently, a rotating mirror or a cam-driven mirror is the present choice for M_1. Such a mirror will provide circular glint motion or linear motion array either of two axes, but not along both independently and simultaneously.

4. Beam/Target Image Monitoring and Data Recording

The monitoring optics diagramed in Fig. 38 provide two types of permanent records of target/beam image data. All experimental activity involving the target will be recorded on video tape along with voice-entered test conditions. Actual glint power (measured by the glint photodetectors) and meteorological data have separate recording devices. The TV recording loop also has a color contour quantizer which assigns a color to each of 12 different intensity levels. When used with the color TV monitor, the relative intensity of different parts of the beam is immediately obvious. The unit also computes the fraction of the total field occupied by any one color so that the beam forming efficiency can be measured (percent of total power in the central lobe, for example).

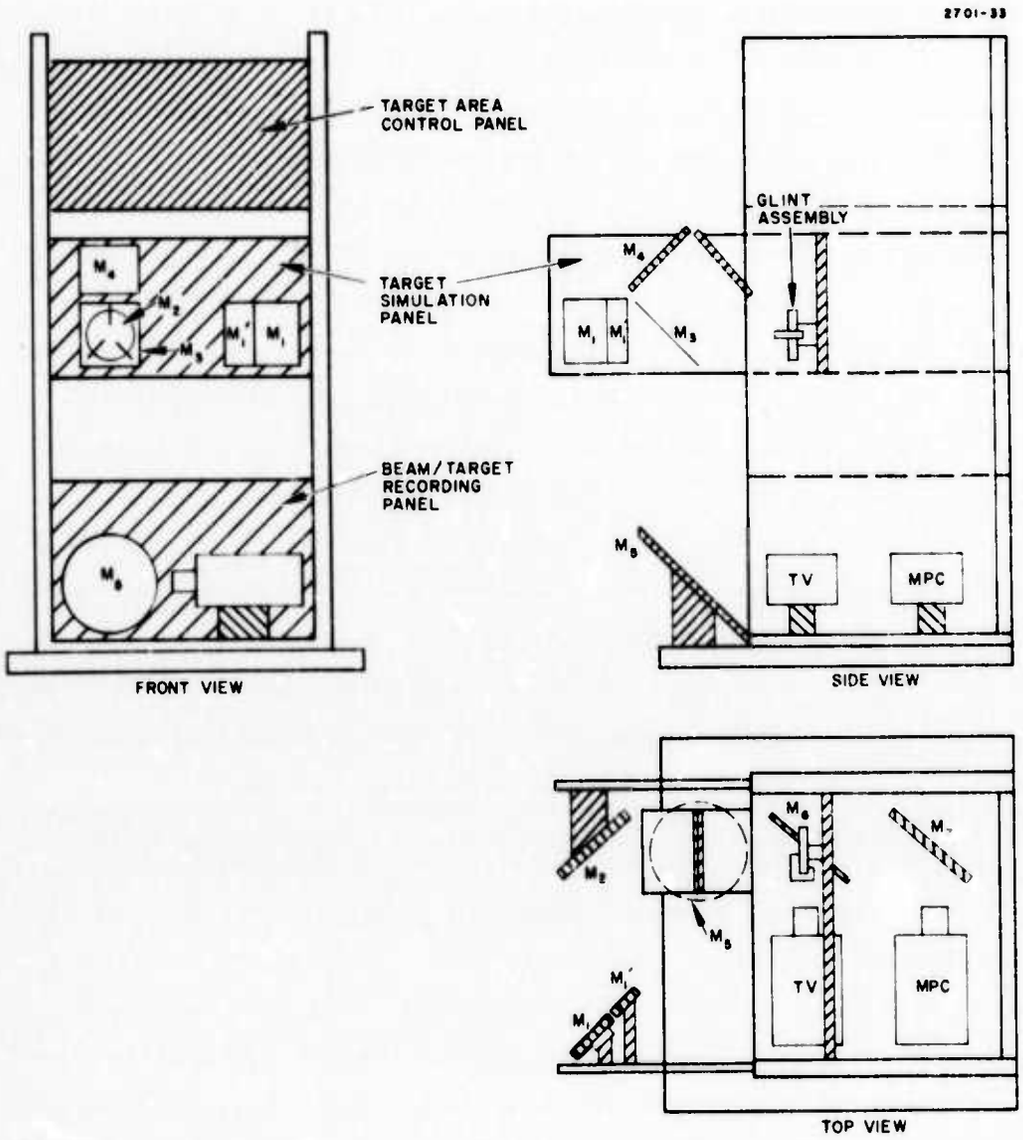

Fig. 37. Target simulator assembly and beam/target diagnostics. See Fig. 38 for definitions of M_1-M_7.

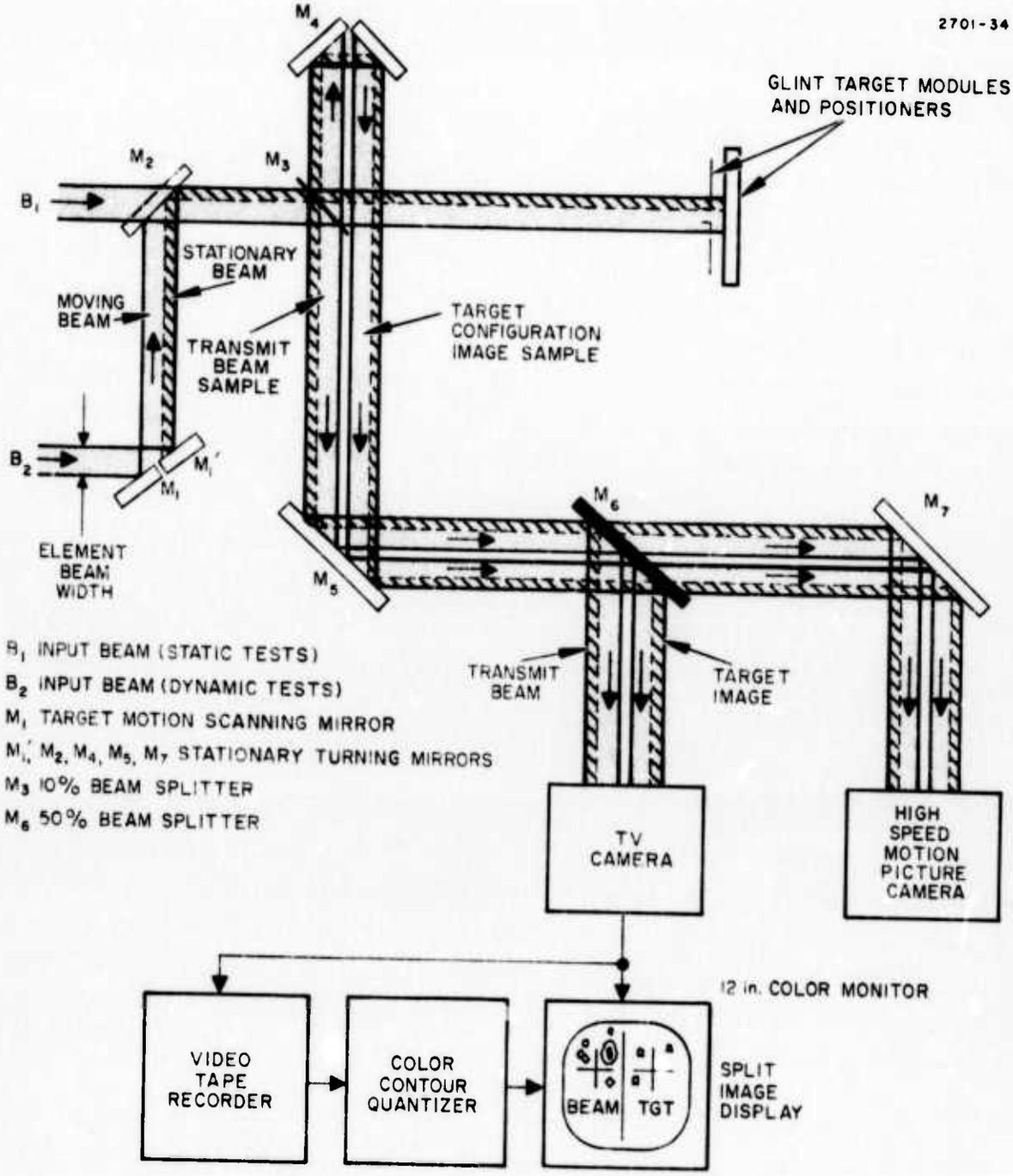

Fig. 38. Beam/target image monitoring optics and recording instrumentation.

The TV camera output is recorded and displayed using a split-screen format. The spatial distribution of the transmitted beam as it appears at the target is displayed on the left half of the screen with the glint positions and relative intensities appearing on the right half. Note that the optics arrangement will always show a stationary target on the TV monitor. Any motion of the incident beam viewed on the left half of the screen will thus be a measure of the error in the COAT system. That is, such motion will indicate the degree to which the system cannot track out atmospheric turbulence or follow target motion.

In addition to the TV monitor, a high speed (350 to 9000 frames/sec) 16 mm motion picture camera (Fastax WF4) can be used where appropriate to record 1 sec test intervals. This instrument will provide much higher time resolution of beam formation than possible with the TV system. For all control loop activities, 6000 frames/sec should be adequate.

As indicated in Fig. 37, all of the monitoring equipment is contained in the rack which houses the target assembly. A view of the monitoring assembly is shown in Fig. 39. The entire target and its monitoring equipment is thus an integral, self-contained package.

G. Propagation Range

The propagation range for the atmospheric tests is located on the roof of building 601 at the Hughes Ground Systems Group (GSG) facility. Figure 40 illustrates schematically the layout of the rooftop range. The COAT system and all control gear for the target and range are located in a laboratory two floors below the roof. The propagation range and the laboratory are connected by a 30 in. diameter periscope.

1. Beam Propagation Path

There are actually four separate propagation paths, each with its own set of periscope mirrors: one for COAT transmit/receive, one for atmospheric monitoring using MTF measurements, and one each for scintillometer transmit and receive (atmospheric monitoring). The scintillometer path includes a mirror mounted near the target assembly for directing the beam back to the receiver. The necessity for this folded-path scintillometer

2701-35

Fig. 39. Photograph of beam/target monitoring panel showing TV camera and high speed movie camera.

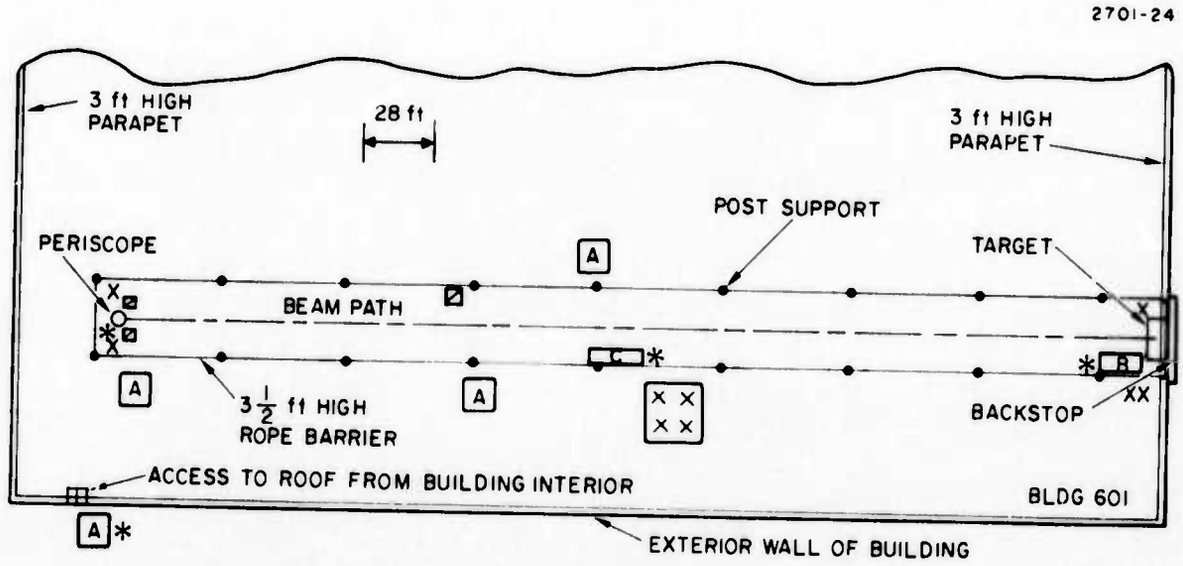

Fig. 40. Rooftop propagation range at GSG facility.

operation is discussed in Section III-G. Figure 41 shows the locations and sizes of the various mirrors as they are seen looking from the target toward the periscope. Each mirror will be independently adjustable and lockable on two axes for alignment and stability.

The periscope itself is mounted on a concrete pedestal connected to the foundation of the building. This was done to decouple the periscope and the mirrors it supports from building vibrations. The output of the periscope is such that the transmitted COAT beam will be 100 cm off the roof. The total beam propagation path is approximately 100 m, 6 m of which is in the periscope.

2. Range Safety

The roof of building 601 has only a single access door which facilitates control of entry onto the propagation range. Although fire regulations prevent the door from being locked, a light will be placed on the inside of the entry door and will automatically come on whenever the main laser of the COAT system is energized. A warning sign will advise anyone entering the roof area of the potential hazard. The sign will also request that anyone going onto the roof obtain permission from the COAT system operators by way of an intercom at the door.

Entrance to the range itself will be blocked off by a 3-1/2 ft high rope fence and the range will be monitored by a TV camera mounted on the periscope. Warning lights and signs are located as shown in Fig. 40 to further remind any personnel on the roof of the potential hazard. There will be three intercom locations on the range, one near the periscope, one by the range monitoring equipment, and one at the target. These units will be voice-actuated headsets to enable hands-free communication with the system operators in the lab.

A 4 ft x 6 ft backstop is located immediately behind the target assembly and is large enough to completely block the COAT beam anywhere within ten array element beamwidths. The backstop is painted with a dull black energy-absorbent paint to minimize reflections. Laser safety glasses will be available for all COAT system personnel will be working either in the laboratory or on the roof during system alignment or operation.

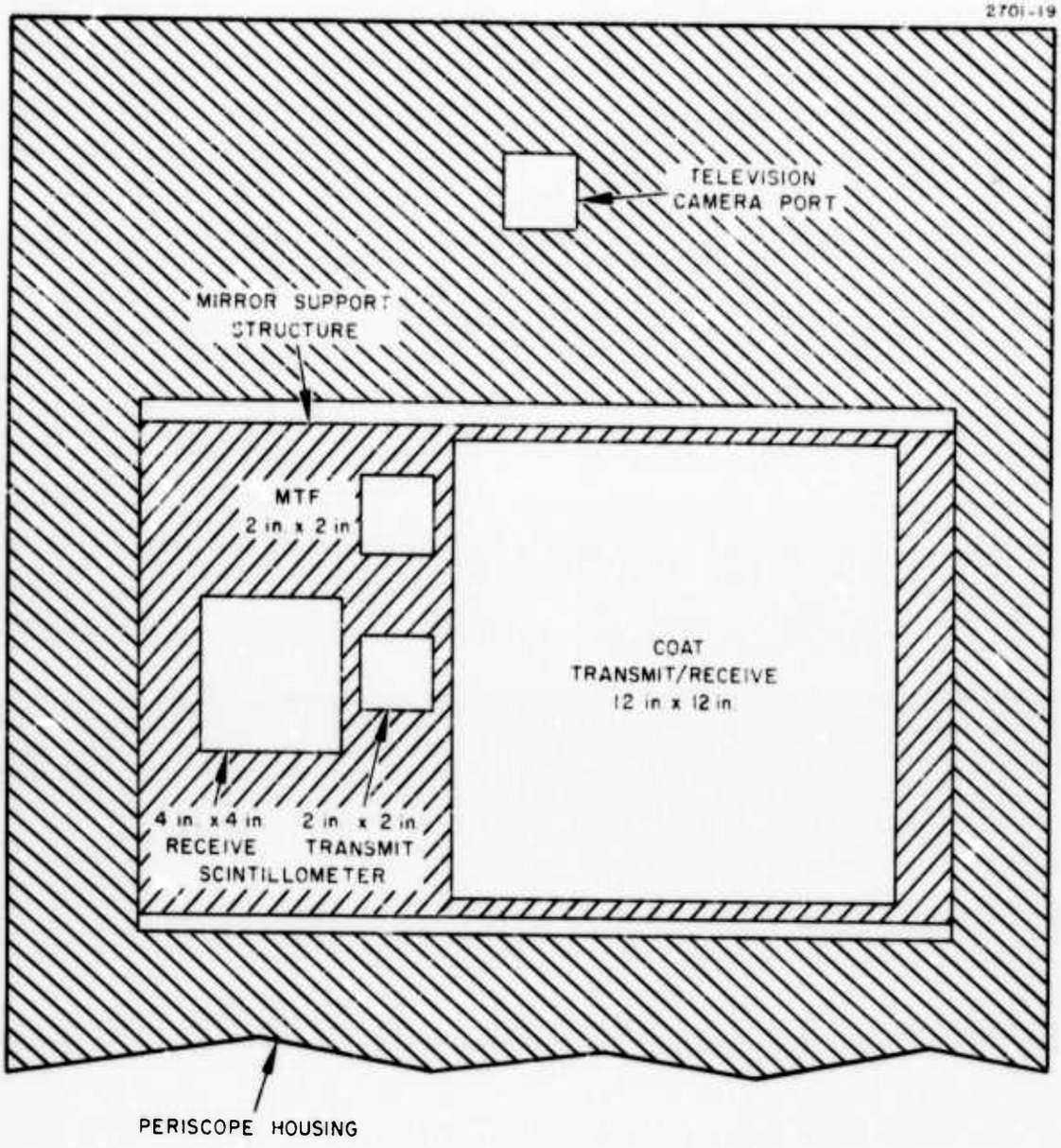

Fig. 41. Periscope as viewed from the target showing various mirror locations and sizes.

3. Atmospheric Monitoring

The atmospheric turbulence on the range is to be characterized by measuring the refractive index structure function constant, C_n. Three instruments will be used to measure C_n: a dual-probe differential microthermometer, an optical scintillometer, and an optical MTF measuring instrument. After conversations with Gerhard Ochs of NOAA, we expect the microthermometer (μT) to provide the most reliable and reproducible values of C_n, particularly in high turbulence, but the scintillometer and MTF were felt necessary as checks on the μT instrument.

A new μT instrument has been fabricated and tested at HRL. A block diagram of the device is shown in Fig. 42(a).* The temperature sensors are simple 5 W, tungsten-filament light bulbs with the glass envelope removed. These probes have a nominal room temperature resistance of 470 ohms. The electronics includes a low-noise preamp, a true-rms measuring unit (Intronics R101), an integrator for averaging the rms fluctuations, and an output to a strip chart recorder. The low frequency cutoff point of the integrator can be selected as 0.17 Hz, 0.017 Hz, or 0.0017 Hz and the integration time constant can be chosen as 1, 10, or 100 sec. The instrument also includes appropriate controls for calibration, gain adjustment, and probe balancing. A photograph of the probe assembly (the bulbs are covered) and the electronics is shown in Fig. 42(b).

An optical scintillometer (OS) has also been constructed and given preliminary tests at HRL. The early tests showed agreement to within a factor of 3 between C_n measured by the μT and the OS. Further refinements of the electronics were required, however, and these have only recently been completed. Figure 43 shows a block diagram of the OS along with a photograph of the transmitter He-Ne laser, 2 mrad FOV optical receiver, and electronics.

*This design is a modified version of that provided by G. Ochs and R. Lawrence at NOAA.

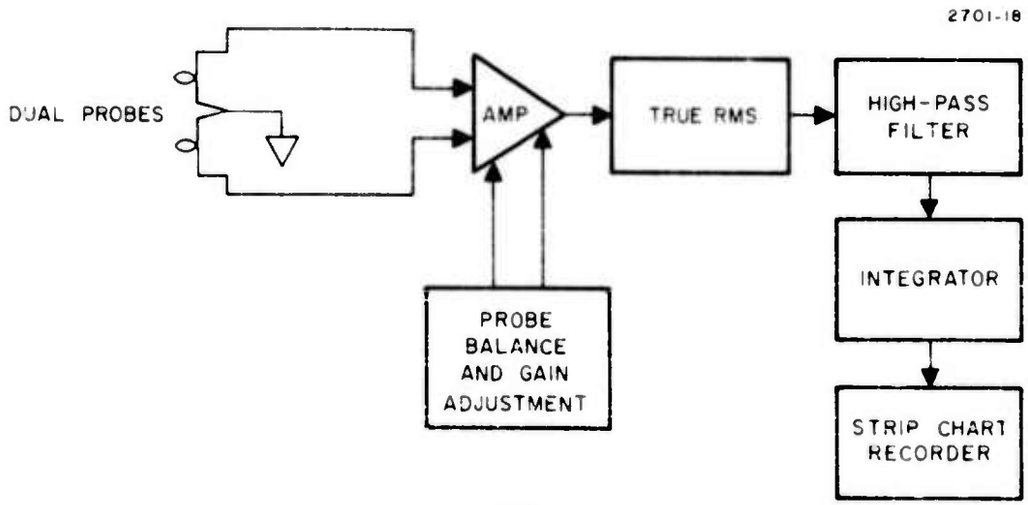

(a)

M10023

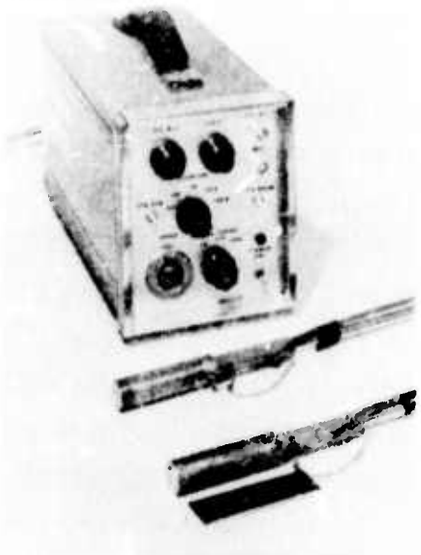

(b)

Fig. 42. Dual-probe differential microthermometer. (a) Block diagram. (b) Photograph showing probes (covered) and electronics.

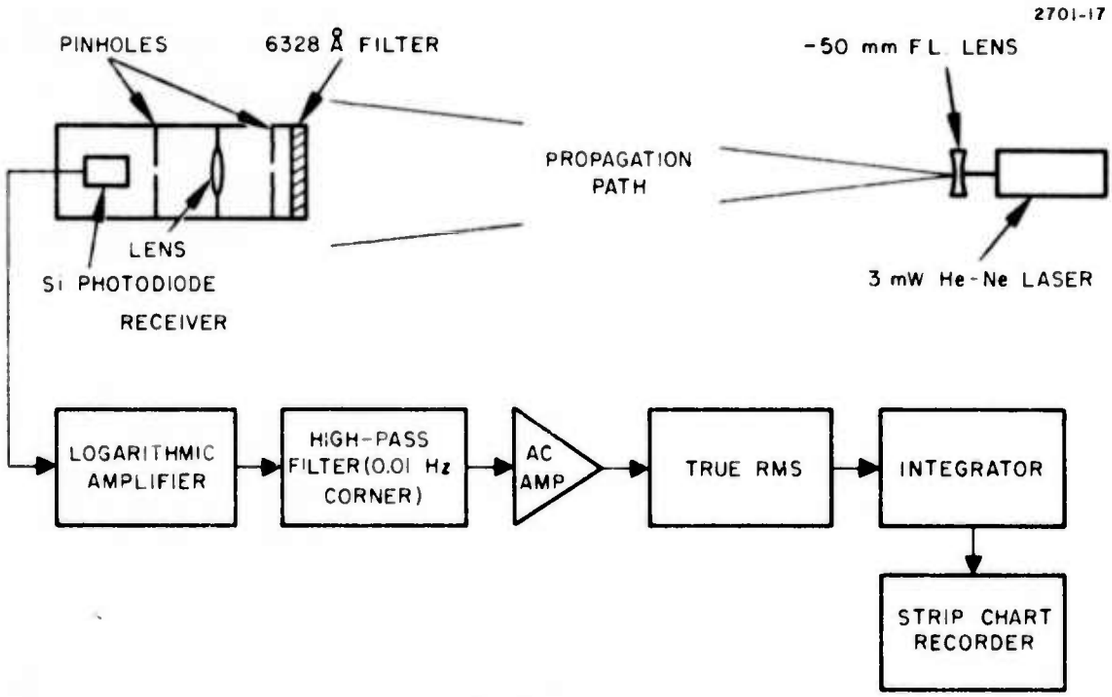

(a)

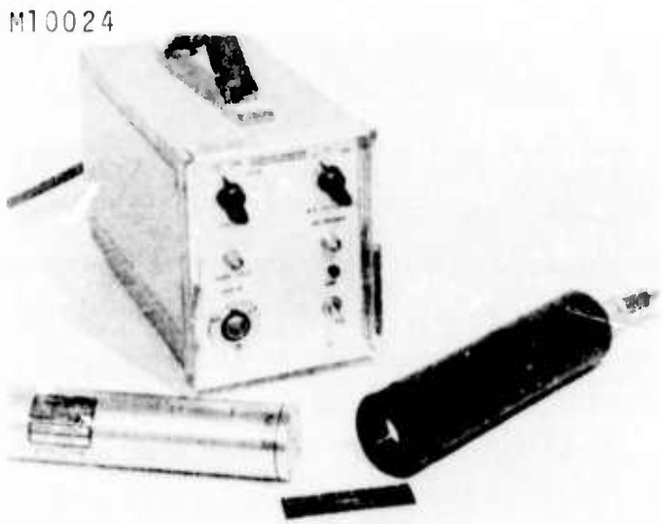

(b)

Fig. 43. Optical scintillometer. (a) Block diagram. (b) Photograph of components (laser, receiver, and electronics).

The accuracy of C_n as measured by the OS will be limited by a number of factors. First, the 100 meter propagation path is too short[1] for validating the assumptions which relate C_n to the rms beam wander at the receiver. A retro-mirror is thus used to double the path length, but 200 meter is still at the lower limit of allowable path lengths for visible wavelengths.[1, 2] Agreement between absolute values of $C_{n(opt)}$ and $C_{n(therm)}$ is not expected to better than a factor of 2, but the two values should follow a predictable relationship as observed by others.[3] Within this relationship (to be determined empirically), $C_{n(opt)}$ and $C_{n(therm)}$ should agree to within 20%.

The other limitations on the accuracy of $C_{n(opt)}$ are optical path saturation at larger C_n values and beam wander introduced by vibrations of the retro-mirror. The former limitation is fundamental and unavoidable; the latter will be minimized by mounting the retro-mirror directly on the load-bearing wall where the target is also mounted, but the amount such mirror vibrations may contribute to the value of $C_{n(opt)}$ has not yet been determined.

The third method of measuring C_n uses a determination of the optical MTF of the propagation path. No measurements have been made with the MTF instrument during this quarter because both the periscope and the MTF device have been undergoing modifications.

4. System-Range-Target Interconnection

Figure 44 shows the location of all the various system components, instrumentation, and recording apparatus. Continuous recording is provided for the microthermometer (ΔT), scintillometers, and meteorological instruments (MET). The latter includes wind velocity and direction, relative humidity, and barometric pressure. The MTF measurements will be made periodically (once per hour) since a continuous measurement is not practical.

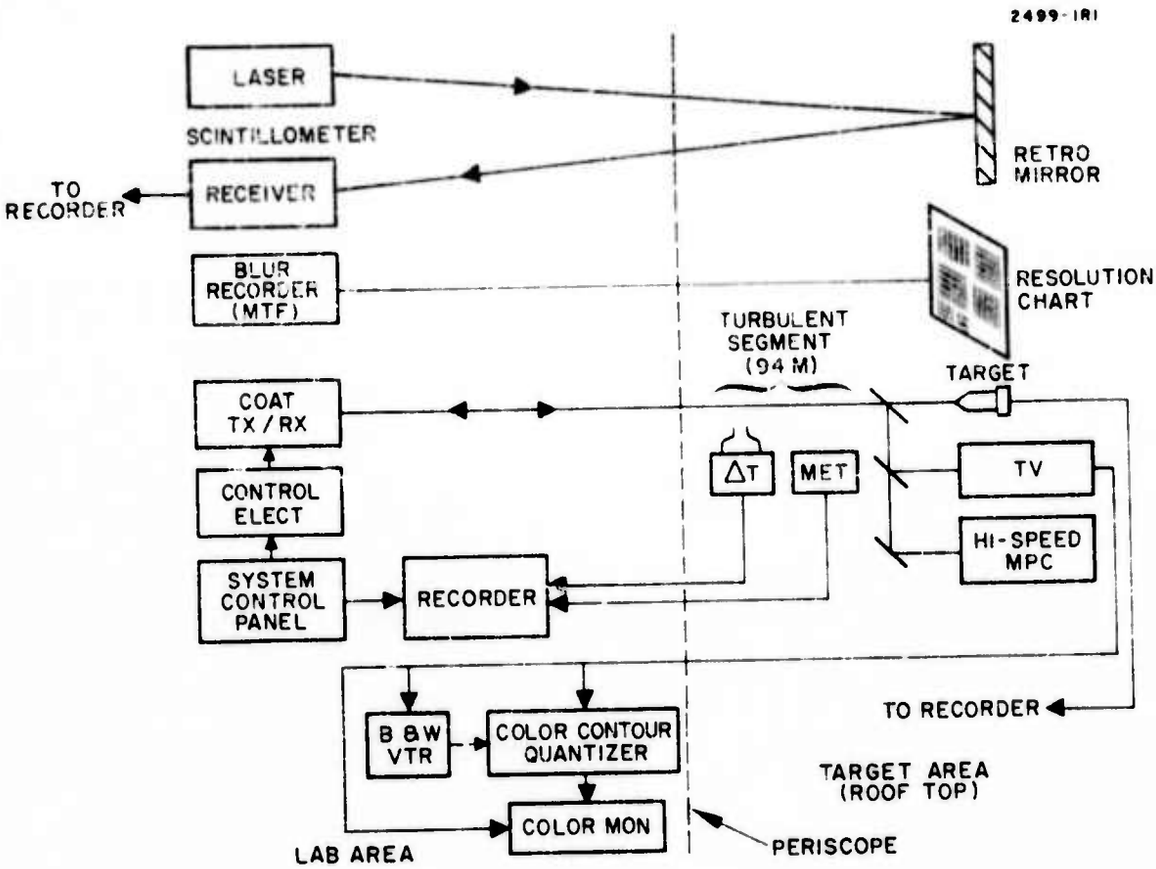

Fig. 44. Locations of instrumentation and recording systems.

IV. MEASUREMENTS PROGRAM

The details of both the calibration and on-range measurements to be performed were given in the first quarterly report. A minimum amount of time will be devoted to calibration as a result of the delayed system completion. All of the range measurements described in the previous report must be made to understand the system performance, but our primary emphasis will be on measurements with moving, multiglint targets.

V. PLANS FOR THE NEXT QUARTER

The third quarter of the program will be devoted primarily to calibration of the visible model and to initial on-range measurements. Simultaneously, however, we will be using the full computer simulation to study the same cases as in the range measurements. These studies will provide additional insights into the system performance in greater detail than possible with the hardware. They will also verify how well the computer code models the hardware performance. These studies have been delayed until the system parameters were finalized and the measurement scenarios more completely defined.

The third quarter will also see the start of Task 3 of the contract: evaluation and design recommendations for a field operational high power planar array. Some of these studies will be based on the performance of the visible model and thus will be delayed until experimental results are available. Other areas of investigation will get under way, including evaluation of first-generation high power components and study of high power planar array configurations. We will also begin preliminary investigations of how to apply multidither COAT to continuous, deformable mirrors.

REFERENCES

1. G. Ochs, private communication.

2. D. L. Fried, J. Opt. Soc. Am. 57, 175 (1967).

3. J. A. Dowling and P. M. Livingston, J. Opt. Soc. Am. 63, 846 (1973).

MISSION
of
Rome Air Development Center

RADC is the principal AFSC organization charged with planning and executing the USAF exploratory and advanced development programs for electromagnetic intelligence techniques, reliability and compatibility techniques for electronic systems, electromagnetic transmission and reception, ground based surveillance, ground communications, information displays and information processing. This Center provides technical or management assistance in support of studies, analyses, development planning activities, acquisition, test, evaluation, modification, and operation of aerospace systems and related equipment.

84